AEDC-TR-69-71

MEASUREMENTS OF LOCAL HEAT-TRANSFER RATE ON A COOLED SHARP FLAT PLATE IN THE MERGED LAYER FLOW REGIME

David E. Boylan
ARO, Inc.

June 1969

VON KÁRMÁN GAS DYNAMICS FACILITY
ARNOLD ENGINEERING DEVELOPMENT CENTER
AIR FORCE SYSTEMS COMMAND
ARNOLD AIR FORCE STATION, TENNESSEE

NOTICES

When U. S. Government drawings specifications, or other data are used for any purpose other than a definitely related Government procurement operation, the Government thereby incurs no responsibility nor any obligation whatsoever, and the fact that the Government may have formulated, furnished, or in any way supplied the said drawings, specifications, or other data, is not to be regarded by implication or otherwise, or in any manner licensing the holder or any other person or corporation, or conveying any rights or permission to manufacture, use, or sell any patented invention that may in any way be related thereto.

Qualified users may obtain copies of this report from the Defense Documentation Center.

References to named commercial products in this report are not to be considered in any sense as an endorsement of the product by the United States Air Force or the Government.

MEASUREMENTS OF LOCAL HEAT-TRANSFER RATE ON A COOLED SHARP FLAT PLATE IN THE MERGED LAYER FLOW REGIME

David E. Boylan
ARO, Inc.

FOREWORD

The work reported herein was sponsored by the Arnold Engineering Development Center (AEDC), Air Force Systems Command (AFSC), under Program Element 65401F.

The results of research were obtained by ARO, Inc. (a subsidiary of Sverdrup & Parcel and Associates, Inc.), contract operator of the AEDC, AFSC, Arnold Air Force Station, Tennessee, under Contract F40600-69-C-0001. The tests were conducted from August through November, 1968, under ARO Project No. VM5915, and the manuscript was submitted for publication on February 24, 1969.

The author wishes to acknowledge the assistance of C. T. Kidd in obtaining the conventional heat-transfer measurements.

This technical report has been reviewed and is approved.

Vincent A. Rocco
2nd Lt, USAF
Research Division
Directorate of Plans
and Technology

Edward R. Feicht
Colonel, USAF
Director of Plans
and Technology

ABSTRACT

Results of measurements of the local convective heat-transfer rate on a sharp-leading-edge flat plate at various angles of attack and in the merged layer flow regime are presented. The measurements were obtained using a phase-change temperature-sensitive paint, which greatly simplifies instrumentation requirements, and these measurements were checked using conventional heat-transfer instrumentation. Data obtained on the windward surface at 0-, 10-, and 20-deg angles of attack are compared to theoretical predictions. The data, which are in the range $0.6 \leq \dot{q} \leq 6.0$ Btu/ft^2-sec, demonstrate the feasibility of utilizing phase-change temperature-sensitive paint in place of conventional heat-transfer instrumentation in low-density high-speed flows. The data at large angles of attack (wedge angles) are shown to correlate in the same manner as the zero angle-of-attack data when local inviscid flow parameters are utilized. Based on local inviscid values, the data are in the Mach number range from 4 to 10 and viscous interaction parameter $\overline{v}_i = M_i(C_i/Re_{i,x})^{1/2}$ range from 0.06 to 0.80. A strong Mach number influence as well as the nonexistence of a definable strong interaction flow regime in this Mach number range was noted. An overshoot over the free molecular flow value was measured although it was not as great as the overshoot in local pressure which has been reported in the literature. Local heat-transfer rate for a given value of $\overline{v}_{i,x}$ in the Mach 10 range is from 50 to 100 percent higher than previously measured values in the Mach 20 range.

CONTENTS

APPENDIXES

I. ILLUSTRATIONS

Figure

Page

NOMENCLATURE

a_c	Thermal accommodation coefficient
C	Chapman-Rubesin viscosity relationship, $(\mu_w/\mu)\ (T/T_w)$
C_1, C_2, C_3	Constants
C_H	Stanton number, $\dot{q}/\rho_\infty u_\infty\ (H_o - H_w)$
c	Specific heat of material
c_p	Specific heat of the gas at constant pressure
E_o	Gage output, mv
H	Enthalpy
h	Convective heat-transfer coefficient, Btu/ft^2-sec-°R
k	Material thermal conductivity, Btu/ft-sec-°R
ℓ	Thickness of sensor
M	Mach number
p	Pressure
Pr	Prandtl number
$\dot{q}$	Heat-transfer rate after steady-state conditions are reached, Btu/ft^2-sec
$\dot{q}_s$	Heat-transfer rate during passage of nozzle shock system over model, Btu/ft^2-sec
R	Sensor radius
Re	Reynolds number
T	Temperature
T′	Temperature difference between heat-transfer gage and model surface

T_i	Initial temperature of the heat-transfer material
T_p	Temperature at which a particular paint is rated to change phase
t	Time
t_p	Time required after step heat input for paint to change phase
U_∞	Free-stream velocity
$\overline{v}$	Viscous interaction parameter, $M(C/Re_x)^{1/2}$
x	Distance from leading edge
y	Distance normal to flat plate
α	Angle of attack
α'	Material thermal diffusivity, ft^2/sec
γ	Ratio of specific heats
θ	Shock angle
λ	Mean free path
μ	Viscosity
ρ	Density

SUBSCRIPTS

aw	Adiabatic wall
FM	Free molecular flow
i	Inviscid flow except when used as T_i
o	Stagnation conditions
SI	Strong interaction
w	Model wall
x	Distance from leading edge of model
y	Distance normal to surface of model, positive inward
∞	Free-stream conditions

SECTION I
INTRODUCTION

Measurements of heat-transfer rates in hypersonic rarefied flows have not been widely attempted. Facilities producing such flows are generally quite small, and the resulting difficulties with model construction and instrumentation tend to discourage attempts at making such measurements. A technique which avoids both of these problems (Ref. 1) has been applied to moderate low-density flows. The purpose of this report is to present an extension of this technique to a more rarefied flow condition and to present data obtained on a cooled sharp flat plate in the merged layer flow regime. A flat plate model was selected because comprehensive experimental studies on flat plates (Refs. 2, 3, and 4) using conventional heat-transfer techniques have been reported. In addition, a large number of theoretical studies have been made in recent years on the idealized flat plate model with emphases on the merged layer flow regime (Refs. 5 through 10).

The results of the present investigation could not be directly compared to much of the earlier experimental work because of a strong initially unsuspected Mach number influence that was found after the present results were analyzed. It was therefore necessary to extend the present investigation and utilize conventional heat-transfer techniques to verify the present measurements.

Briefly, the present technique involves using temperature-sensitive paint, motion-picture time histories, and the one-dimensional heat conduction equation to obtain aerodynamic heating rates at specific positions on the test model. The relative ease of this technique compared to conventional instrumentation techniques indicates the possibility for applications in many aerodynamic studies in the low-density flow regime. The paint utilized undergoes a phase change (solid to liquid) as it heats rather than only changing color as do paints more often used in such applications.

SECTION II
THE MERGED LAYER

A typical schematic of the flow over the surface of a sharp flat plate in hypersonic rarefied flow is shown in Fig. 1, Appendix I. The strong and weak viscous interaction regimes downstream of the merged regime are discussed fully by Hayes and Probstein (Ref. 11). Upstream of the

merged layer regime a kinetic approach must be used in analysis of the flow. The length of the kinetic flow regime and the transition to the merged layer regime are not well defined at the present time.

The merged layer regime itself can be described simply as that portion of the flow field in which the shock wave merges with the viscous layer. However, the theoretical treatment of the flow within the region has proved to be quite difficult. Theoretical analyses have undergone a rather evolutionary process in which there is a distinction between those that preceded experimental work and later ones which followed some detailed flow field measurements (Refs. 12, 13, and 14). Recent theoretical publications (e. g., Refs. 5 through 10) are the most applicable in the present discussion, and brief comments on some of these follow.

The recent work of Cheng et al. (Ref. 5) utilizes a finite-difference solution to the Navier-Stokes equations with the assumption of a thin boundary layer and a thin shock. In the region $0.1 \leq \overline{v}_{\infty, x} \leq 0.8$, calculated values of heat transfer are from 10 to 100 percent higher than available high Mach number data. The strong shock assumption ($M_\infty >> 1$) is also made in this analysis, and numerical results reported in Ref. 5 are limited to one particular flow condition which is not approximated in the present case.

Shorenstein and Probstein (Ref. 6) also approach the leading-edge problem from a continuum viewpoint. In addition to the Navier-Stokes shock structure assumption, shock curvature, slip, and temperature jump effects are taken into account. Heat-transfer results compared to experimental results at high Mach numbers are in very good agreement in the range $0.1 \leq \overline{v}_{\infty, x} \leq 1.0$. A correlation parameter expressed as $(T_W/T_O)^{1/2}(\overline{v}_{\infty, x})^2$ also is used which allows empirical correlation of their numerical results with heat-transfer measurements.

Chow (Ref. 7) combines the Navier-Stokes equations in the shock wave region with a cubic-parabolic slip-velocity profile in the boundary-layer region. It is assumed that both regions have the same velocity and velocity gradient along their common boundary. Comparison of several flow field and surface measurements to the numerical results are quite favorable. Although no heat-transfer results are shown in Ref. 7, Chow's computer program has been made available to the author and direct comparisons are made to the results of the present investigation.

Another continuum approach has been published by Rudman and Rubin (Ref. 8). Their analysis is applicable for $M_\infty \geq 2$, and includes

consideration of flat plates at angle of attack. Comparison of heat-transfer results, which are forced to fit $C_H)_{FM}$ at the leading edge, to high Mach number experimental results is good for $\overline{v}_{\infty, x} \leq 2.0$. Rudman and Rubin indicate a very strong Mach number effect on C_H, in the range $15 \leq M \leq 50$, for a given value of $\overline{v}_{\infty, x}$. Their results have been extrapolated to $M_\infty = 10$ to compare to the present experiment.

A kinetic theory approach was used by Huang and Hartley (Ref. 9). The Boltzmann equation with the BGK model is used to calculate flow field and surface conditions. The numerical results were restricted to the case of $M_\infty = 1.5$, because of limited computer storage capacity. Comparisons made with heat-transfer results obtained at high Mach numbers were quite good although probably fortuitous since the calculations were performed for entirely different conditions. Similar comparisons of skin friction and surface pressure were qualitatively adequate, but significantly different absolute values appear because of this reason.*

A Monte Carlo direct simulation technique was recently reported by Vogenitz et al. (Ref. 10). Their study provides a detailed description of the flow near the leading edge. Effect of Mach number, plate length, and wall temperature were studied. This study, in common with many others, is restricted to monatomic gases. However, the liberty of comparing it with the present measurements is taken.

All of these recent theoretical analyses are compared to the present results. However, it should be noted that only the results of Refs. 7 and 8 can be directly compared for the reasons given above.

SECTION III
APPARATUS AND PROCEDURE

The data were obtained using the arc-heated, low-density, hypersonic tunnel (Gas Dynamic Wind Tunnel, Hypersonic (L)), located at the von Kármán Gas Dynamics Facility (VKF).

3.1 WIND TUNNEL

Tunnel L, shown in Fig. 2, is a low-density, hypersonic, continuous-type, arc-heated, ejector-pumped facility, normally using nitrogen or

*This work was recently extended to hypersonic flow (AIAA paper Re-63) but no heat-transfer calculations were reported.

argon as the test gas and consisting of the following major components, in streamwise order:

1. Continuous, water-cooled, d-c arc heater, Thermal Dynamic F-40 or U-50, both modified slightly, with a 40-kw selenium rectifier power supply. Gas is injected without swirl in the F-40 arc heater and with or without swirl in the U-50 unit. Unless otherwise noted, all testing is done without use of swirling gas injection.
2. Cylindrical, water-cooled settling section of variable size, but normally of 3-in. diameter and 6- and 10-in. length.
3. Axisymmetric, aerodynamic nozzle, variable sizes with 0.10- to 1.20-in. -diam throats and 2.0- to 8.2-in. -diam exits. Three contoured nozzles having no flow gradients in the test section are currently available, in addition to older conical nozzles.
4. Cylindrical test section tank of 48-in. diameter surrounding the test section and containing instrumentation, cooling water connections, and probe carrier.
5. Axisymmetric diffuser with interchangeable components for varying test conditions. Convergent water-cooled entrance, constant-area throat, and divergent exit sections.
6. Water-cooled heat exchanger.
7. Isolation valve.
8. Air ejector of two stages.
9. Connection to the VKF, evacuated, 200,000-ft^3, spherical vacuum reservoir and its pumping system.

All critical components of the tunnel and related system are protected by backside water cooling. The two-stage ejector system is driven by air instead of steam because of the ready availability of high pressure air at the tunnel site. Although the working gas is normally nitrogen or argon, other gases may be used. The first published description of this tunnel was that of Potter et al. (Ref. 15).

3.2 TUNNEL CALIBRATION

Gas flow rate to the arc heater is measured through use of calibrated sonic-flow orifices, and reservoir pressure is measured with a Consolidated Electrodynamics Corporation Electromanometer®. Inaccuracies of these systems, on the basis of comparison with other means

of measurement, and repeatability, are estimated to be less than ±0.5 percent for both flow rate and reservoir pressure.

Total enthalpy at the nozzle throat is determined by use of a calorimeter which, on the basis of comparison with other results and repeatability, appears accurate to within ±4 percent limits of error. The measurement is supplemented by a probe system which measures local total enthalpy and mass flux in the test section with an estimated error limit of ±2 percent for mass flux and ±5 percent for enthalpy.

Impact pressures are measured with variable-reluctance, differential pressure transducers and water-cooled probes. Calibration of the transducers is accomplished by means of an oil-filled micromanometer and a McLeod gage. Inaccuracy in impact pressure measurement is believed not to exceed ±2-percent limits. Static pressures are measured by the same method but are not used for primary calibration purposes because of the very large corrections for viscous and rarefied flow phenomena.

The establishment of reservoir conditions, determination of impact pressures, and proof of inviscid, adiabatic core flow through the nozzles form part of the flow calibration. This information is used in a calculation which accounts for nonequilibrium expansion of the gas throughout the nozzle to yield the needed flow properties.

3.3 NOZZLE FLOW CONDITIONS

Two separate contoured nozzles, having no radial or axial gradients in the test region, were used during the test. The stagnation conditions were such that the assumption of the flow being vibrationally frozen from the sonic point is justified. General information on the undisturbed flow properties in the test region is given in Table I, Appendix II. A description of the design and calibration of the contoured aerodynamic nozzles is given by Potter and Carden (Ref. 16). The tunnel calibration was checked immediately before and after the present investigation.

3.4 TEST MODELS AND COOLING SHOE

Two water-cooled sharp-leading-edge flat plates were designed for utilization of the phase-change temperature-sensitive paint technique and conventional heat-transfer instrumentation. Figure 3 indicates pertinent dimensions, and Fig. 4 is a photograph of both models showing the chordwise heat-transfer element and conventional instrumentation.

It was necessary to ensure that no heat load was being applied to the model during the time in which flow conditions were being established. A water-cooled shield or shoe was therefore constructed which could be removed by remote control when data acquisition was desired. Figure 5 is a photograph of the shoe in place around the model. Flow blockage resulted when the shoe was placed in the nozzle test region. However, flow was quickly reestablished when the shoe was removed. Discussion of the influence of this transient portion of the flow is given in Section 4.1.1. Lower surface wedge angle was kept at 16°43', and the leading-edge radius was less than 0.001 in. to avoid difficulties associated with failure to approximate the "sharp slender" assumptions made in theoretical analyses. This problem is discussed in Ref. 13.

3.5 HEAT-TRANSFER ELEMENT

The selection of the proper material on which to obtain measurements by temperature-sensitive paint depends on the flow conditions to which the model is subjected, the operating temperature of the material, the level of the heat flux, and the thermal and mechanical properties of the heat-transfer material. The accurate knowledge of the thermal properties is the most important criterion of these factors. A material of low conductivity, high operating temperature, and low thermal diffusivity is required. In addition, the material should have a dark surface color, be easily machinable, and easily obtainable. Quite a few materials such as alumina ceramics, fiber glass-reinforced plastics, lava, graphites, Lexan , nylon and Teflon meet many but not all of these requirements. Lexan®, nylon, and Teflon® meet many but not all of selection for the present application. Table II gives the physical properties of these materials. The data obtained using the Lexan material proved consistently poorer than either nylon or Teflon because of the poor resolution of the film as phase change occurred. For this reason data obtained with Lexan as the heat-transfer material are omitted. Future investigations in which a dark background may be provided for better film resolution could utilize this material which is far superior to either nylon or Teflon in its machining characteristics.

It can be observed in Fig. 3a that the heat-transfer element was placed in the flat plate model starting at a position 0.25 in. from the leading edge. This was necessary to prevent conduction from the metal to the heat-transfer element and to avoid leading-edge ablation. A thermocouple was placed at the bottom of the heat-transfer material as shown in Fig. 3a. The initial temperature of the material and evidence of the lack of significant conduction from the flat plate to the heat-transfer element were obtained from monitoring this thermocouple.

3.6 CONVENTIONAL INSTRUMENTATION

Model B, shown in Figs. 3 and 4, was instrumented with three different types of conventional heat-transfer gages, including a steady-state Gardon gage, a transient slug calorimeter, and a platinum thin-film resistance thermometer. The latter two types were constructed and tested when results of the Gardon instrument indicated that the initial heat pulse resulting from the blockage of the flow by the heat-transfer shoe may have affected the phase-change paint data. The small size of the model allowed only one gage to be installed in the model at a time. The other two instrumentation ports were plugged to prevent flow through the model. In addition, it was not possible to instrument the model closer than 1.20 in. from the leading edge. Table III lists physical properties and calibration factors for these gages. Having only one instrumentation channel obviously limited the amount of data obtainable using conventional techniques. Data reduction theory and factors affecting the accuracy of both the phase-change paint and conventional heat-transfer data are discussed in Section IV.

3.7 TEST PROCEDURE

The flat plate model was positioned on the nozzle centerline normal to the tunnel window a short distance downstream of the nozzle exit at an angle of attack of 0, 10, or 20 deg. For the phase-change paint investigation small spots of temperature-sensitive paint about 0.070 in. in diameter were lightly painted on the surface of the heat-transfer material at random distances from the leading edge. The water-cooled heat-transfer shoe was then positioned around the model, the tunnel evacuated, and flow initiated. When steady-state conditions were obtained a delay circuit was activated which started a 16-mm motion-picture camera equipped with black and white film and operating at 24 frames per second. Three seconds after the camera started, the cooling shoe dropped and a strip-chart recorder monitoring the thermocouple embedded in the heat-transfer material started. The flow was terminated when it was observed that the paint had changed from a solid to a liquid state. The heat-transfer element was then cleaned with a solvent and the procedure repeated for other conditions. The model was illuminated with a photoflood lamp. The procedure using conventional heat-transfer gages was very similar except the data acquisition system was much more complex and there was no need for the motion-picture record.

SECTION IV
DATA REDUCTION THEORY AND RESULTS

4.1 PHASE-CHANGE PAINT DATA

The use of temperature-sensitive phase-change paint in conjunction with a time history required for the phase change to occur allows quantitative measurement of heat flux to be obtained. The data reduction is based on the one-dimensional heat conduction equation for a semi-infinite slab expressed as

$$\frac{\partial T}{\partial t} = \alpha' \frac{\partial^2 T}{\partial y^2} \tag{1}$$

where

$$\alpha' = k/\rho c \tag{2}$$

and y is normal to the plate surface. The initial and boundary conditions are:

$$\left.\begin{aligned} T(\infty,t) &= T_i \\ T(y,0) &= T_i \\ \frac{\partial T}{\partial y}(0,t) &= [T_{aw} - T(0,t)]\frac{h}{k} \end{aligned}\right\} \tag{3}$$

The first two of these conditions simply states that the material is subjected to a step heat pulse at t = 0 and that the temperature of the material remains undisturbed at an infinite distance below the surface. The last statement requires that the heat flux leaving the gas at the surface equals the flux into the solid material.

Several other assumptions are implicit in this data reduction method as follows:

1. The surface of the material is at the same temperature as the paint when phase change occurs.
2. The thermal properties of the material (α', k) are invariant over the temperature range in question.
3. The paint does not alter the properties of the material.
4. The variation of temperature in the heat-transfer element parallel to the flow direction is small compared to the variation normal to the surface so that the heat flux can be assumed to be one-dimensional.

The solution of Eq. (1) is discussed in Ref. 17 and, at the surface where y = 0, may be expressed as

$$\frac{T_p - T_i}{T_{aw} - T_i} = 1 - e^{\frac{h^2}{k^2} \alpha' t_p} \operatorname{erfc}\left[\frac{h}{k}\sqrt{\alpha' t_p}\right] \tag{4}$$

Assuming that thermal properties of the material are known and that an accurate measurement of time for a particular paint to reach the rated temperature at which phase change occurs is made, the only unknown in Eq. (4) is the convective heat-transfer coefficient, h related to $\dot{q}$ by:

$$h = \dot{q}/(T_{aw} - T_w) \tag{5}$$

where

$$T_w = T_p$$

and

$$T_{aw} = \frac{U_\infty^2}{2gc_p}\sqrt{Pr} + T_\infty \tag{6}$$

A Prandtl number of 0.7 was assumed in the present case. A dimensionless heat-transfer coefficient or Stanton number may be expressed in the usual manner as:

$$C_H = \dot{q}/\rho_\infty U_\infty (H_o - H_w) \tag{7}$$

Equation (4) may be easily integrated in a graphical manner as was done in Ref. 1. Figure 6a is a typical graphical solution of Eqs. (4), (5), and (7) for a particular material, flow condition, and initial temperature. Since a rather large number of curves would be necessary to account for variation of T_i and T_p, curves such as Fig. 6 are more useful for selection of the proper paint and material rather than accurate data reduction. Since most available data published are in the form of C_H or some derivation of this parameter, and since the film readout equipment used was capable of punching International Business Machines (IBM) data cards, a data reduction program was written for the Control Data Coporation (CDC) 1604-B computer located in the VKF.

Since the solution of Eq. (4) requires a semi-infinite boundary condition to be maintained, there is a certain thickness of heat-transfer material which must be maintained in order to approximate the "undisturbed" condition at the bottom of the material. The use of back-side water cooling is believed to have effectively eliminated heat transfer into the heat-transfer element from other than convective sources. A thermocouple embedded in the material as shown in Fig. 3a confirmed this, although its location made it more likely to reflect conduction from

the bottom of the model and a small temperature rise was noted. The general solution of Eq. (1) is given in Ref. 17 and, in the present nomenclature, is:

$$\frac{T_y - T_i}{T_{aw} - T_i} = \operatorname{erfc}\left[\frac{y}{2\sqrt{a't}}\right] - \exp\left[\left(\frac{h}{k}\sqrt{a't}\right)\left(\frac{y}{\sqrt{a't}} + \frac{h}{k}\sqrt{a't}\right)\right] \operatorname{erfc}\left(\frac{y}{2\sqrt{a't}} + \frac{h}{k}\sqrt{a't}\right) \quad (8)$$

This equation reduces to Eq. (4) when y = 0.

Equation (8) was calculated at $\dot{q}$ = 1.0 and 5.0 Btu/ft^2-sec for Teflon material, the 10 N_2 nozzle flow condition, and with y = 0.25 in. The results are shown in Fig. 6b and indicate that over the range of test time and $\dot{q}$ experienced during the present investigation, only very small increases in the bottom surface temperature could be expected. The lower time limit of 5 sec was determined by considerations discussed in Section 4.1.1 and the approximate upper limit of 20 sec was determined by the proper selection of paint temperature rating. The heating rate of 5 Btu/ft^2-sec was the approximate upper limit measured and would correspond to measurements nearest the leading edge of the model at 20-deg angle of attack. All other measurements were considerably below this value. Selecting nylon material and/or another aerodynamic nozzle would give essentially the same results as those shown in Fig. 6b.

As explained earlier, a light coating of a particular paint was placed at discrete intervals along the length of the heat-transfer element. Quite often it was necessary to use a particular temperature-rated paint over a portion of the model and a different paint over the remainder. A photographic history showing the cooling shoe falling from the model and each individual paint spot changing from a solid to a liquid was made. Figure 7 shows a small portion of one such photographic record. The film was read on a Benson-Lehner® Model 29E film reader which provided readouts of frame number, distance from the leading edge, and constants for data reduction purposes such as T_i, material, and T_p and recorded these values on IBM data cards. The data could then be directly fed into the data reduction program which calculated values of h, $\dot{q}$, C_H, and various flow parameters.

Data were obtained using the three materials listed in Table II of which only nylon and Teflon produced satisfactory results for reasons given earlier. Rated paint temperature, T_p, varied from 200 to 500°F. Data were obtained on the compression surface of the flat plate at

angles of attack of 0, 10, and 20 deg. Figure 8 presents the results of these measurements in terms of C_H and $\bar{v}_{\infty,x}$. Comparison with theory in Fig. 8 is limited to the strong interaction and free molecular flow theory and the large wedge angle theory of Cheng et al. (Ref. 2). The zero angle-of-attack data in Fig. 8a fall significantly above strong interaction theory in the range $0.1 \leq \bar{v}_{\infty,x} \leq 0.3$ and only drop slightly below this prediction at values of $\bar{v}_{\infty,x} > 0.3$. This does not agree with earlier experimental work in the same range of $\bar{v}_{\infty,x}$ at higher Mach number flow conditions (Refs. 2, 3, and 4). A small but noticeable difference in the level of C_H between the data obtained in the 9 N_2 and 10 N_2 nozzles can also be seen. The difference in wall temperature between these two flow conditions is in the correct direction to account for this increment. A slight overshoot above $C_H)_{FM}$ can be seen in Fig. 8a. One advantage in using this technique for obtaining heat-transfer measurements is the knowledge of T_w (i. e., T_p) explicitly. This value is often not known to the required accuracy in experiments in the merged layer regime. Data obtained at angles of attack of 10 and 20 deg are compared to the strong shock wedge theory of Cheng et al. (Ref. 2) in Figs. 8b and c. Once again, the present data are somewhat above the theoretical prediction. Cheng's theory is not sensitive to the present variation in Mach number and wall temperature and the data do not appear to reflect any such dependence as was the case at zero angle of attack.

The data shown in Fig. 8 do not indicate any consistent variation with T_p but do indicate a slight effect of material. The data obtained with nylon as the element material are consistently lower than those obtained with Teflon. This is probably because of inaccurate knowledge of the material thermal properties or their variation over the present operating temperature range.

4.1.1 Sources of Error

In addition to the obvious necessity of accurate thermal properties, several other sources of error must be considered. Errors in measurement of T_i, T_p, and t_p can affect the accuracy of the data to a large extent in certain cases. The measurement of T_i was made to an accuracy of ±1°F at the beginning of each run. However, this measurement was made before the dropping of the cooling shoe and did not reflect the transient heat pulse on the surface of the model caused by the nozzle shock system passing over the model as flow was being established. Conventional heat-transfer measurements gave this heat-transfer rate and allowed an estimate of this error to be made. The

effect of this short heat pulse is to raise the required values of T_i and shorten the value of t_p in the data reduction program. Measurements of the heat-transfer rate, $\dot{q}_s$, during the shock passage are shown in Fig. 9. The time required for the shock system to pass a given area covered by the phase-change paint could also be estimated from these conventional heat-transfer measurements and is believed to be about 0.035 sec for the 10 N_2 nozzle and 0.020 for the 9 N_2 nozzle. Using the experimentally observed heating rates shown in Fig. 9, and a given value of time, Eq. (4) can then be solved for T_p. Since $T_p = T_w$, this calculation indicates the magnitude of the temperature rise caused by the passage of the shock system. The results are shown in Fig. 10. A very large temperature rise attributable to $\dot{q}_s$ at the surface is calculated at the higher heating rates. The effect of this "effective" error in T_i for a particular material and flow condition is a function of T_p as shown in Fig. 11. Fortunately, for the cases where the model experienced a high value of $\dot{q}_s$ (Fig. 9), a paint with a high value of T_p was also necessary to ensure the proper timing sequence. This drastically reduced the error attributable to the failure to produce a step heating rate. The present measurements in the 10 N_2 nozzle could be a maximum of about 20-percent high at α = 20 deg from this source of error. The data obtained at 0 and 10 deg should be within 10 percent with the present measurement again being on the high side. Measurements in the 9 N_2 nozzle could not be more than 15 percent high with most of the data being within 5 percent of the calculated value using measured T_i. Later comparisons with conventional gage measurements will indicate that the accuracies stated above are on the pessimistic side.

The measurement of the time span t_p for phase change to occur was easily made by utilization of the film reader. A maximum error of ±0.5 sec is thought to be possible with an error of ±0.1 sec being more probable. The effect of a half-second error in the measure of time is shown in Fig. 12. For times greater than 5 sec, the error resulting from this problem was small. Care was taken to utilize paints which did not change phase in less than 5 sec and all of the data reported herein were in the interval $5 \leqq t_p \leqq 20$ sec. Experience indicated that any error in measuring t_p was likely to result in a measured time being greater than true t_p. This would result in a low value of C_H, thereby tending to offset the error resulting from the passage of the starting shock system over the model. The effect of the time span being displaced a maximum of 0.035 sec because of the shock passage can be neglected. The manufacturer's rating of T_p for a particular paint is ±1 percent. This margin of error would yield very small errors in measured heat-transfer rates and can also be neglected. The model positioning technique used to adjust angle of attack was not accurate to

more than ±1 deg. An analysis of the results indicated that a ±5 percent error in C_H or $\dot{q}$ could result from this source of error. Some of the data scatter can no doubt be attributed to this.

4.2 CONVENTIONAL MEASUREMENTS

For a steady-state, long-duration facility such as Tunnel L, a heat-transfer device such as a Gardon gage (Ref. 18) is ideally suited with only gage and model size presenting difficulties in obtaining accurate data. A small, blackened constantan foil, which in the present case was 0.150 in. in diameter and 0.001 in. thick, is soldered around its circumference to a block of copper which acts as a constant-temperature heat sink. The energy absorbed by the foil flows radially to the copper block and as a result, the temperature at the center of the foil rises above that of its circumference. A copper wire attached to the center of the foil completes a thermocouple consisting of the copper wire, the constantan foil, and the copper block. The electromotive force (emf) generated by this temperature gradient is directly proportional to the heating rate incident on the sensor and is expressed as

$$\dot{q} = \frac{4k\ell\, E_o}{R^2 C_1} = C_2 E_o \tag{9}$$

The rise time to 63 percent of final output is:

$$\tau_{63} = \frac{c\,\rho R^2}{4k} = \frac{R^2}{4a'} \tag{10}$$

A standard radiation heat source was used to determine the constant C_2 in Eq. (9). Table III gives this constant with other properties of the Gardon gage. Since the time constant for this particular gage is relatively large, its application to a transient measurement is not possible. However, for a steady-state ($\dot{q}$ = constant) application, the Gardon gage is convenient to use since $\dot{q}$ is directly proportional to transducer output. It was originally planned to use only the Gardon gage to verify the phase-change paint data. However, results such as shown in Fig. 13 indicated that additional measurements were necessary. The emf-time trace shown in this figure allows very good resolution in determining $\dot{q}$ but is inadequate for determining the magnitude or duration of the short energy pulse, $\dot{q}_S$. This transient follows the cooling shoe dropping and is the result of the nozzle shock system being reestablished downstream of the model. Preliminary calculations and estimates of $\dot{q}_S$ from the Gardon gage data indicated that the phase-change paint data may have been influenced by this heat pulse on the surface of the model. Accurate

measurements of $\dot{q}_s$ were obtained from use of a slug calorimeter and a thin-film resistance thermometer. The results of these measurements have already been discussed in Section 4.1.1 and shown in Fig. 9. Both gages were substantially faster in response than the Gardon gage. Calibration of these gages was also made using a standard radiation device. Table III lists characteristics of these two heat-transfer devices in addition to the Gardon gage. A typical emf-time trace is shown in Fig. 14. The time in which the shock system was influencing a particular spot of paint was estimated from traces such as this, assuming a direct relationship between the area of the painted surface and the sensing area of the calorimeter gages. This time was about 0.035 sec in the 10 N_2 nozzle and 0.020 sec in the 9 N_2 nozzle for all angles of attack and axial positions. Both $\dot{q}_s$ and $\dot{q}$ were measured with the slug calorimeter and thin-film resistance thermometer. It can be shown that conduction losses severely affect the results of a slug calorimeter if the elapsed test time is large. For the present application a loss factor of 3 percent for the measurement of $\dot{q}_s$ and 7 percent for $\dot{q}$ was calculated. The slug calorimeter data reported herein have been corrected for this error.

A direct comparison of $\dot{q}$ measured with the conventional instrumentation techniques and $\dot{q}$ derived from the phase-change paint method is shown in Fig. 15. The agreement in the range of overlap ($1.2 \leq x \leq 1.8$ in.) for each angle of attack and flow condition is generally very good. Since the passage of the shock over the surface of the model would not affect the measurement of $\dot{q}$ by the conventional techniques, this possible source of error in the phase-change paint data appears to be less serious than was initially believed possible. This apparent anomaly between the statements made in Section 4.1.1 and the results shown in Fig. 15 is probably caused by an overestimation of the time during which the shock system was affecting a particular spot of paint. Of the three different conventional methods used, the Gardon gage should be more accurate in the present application. In general, the phase-change paint data are more consistent than the conventional measurements. When consideration is also made of the relative ease and complete model instrumentation which is possible using phase-change paint, the advantages of using this technique are clear.

SECTION V
COMPARISON WITH THEORETICAL PREDICTIONS

5.1 ZERO ANGLE-OF-ATTACK DATA

Numerical calculations for local heat transfer at the exact flow conditions of the present test are meager. However, comparison with

available numerical results at other flow conditions provides a qualitative check on the present results. Figure 16 compares the zero angle-of-attack data with the results of Refs. 5 through 9 as well as strong interaction and free molecule flow predictions. The strong interaction calculation was taken from Shorenstein and Probstein (Ref. 6) expressed as

$$C_H)_{SI} = (0.368\, T_w/T_o + 0.0684)\,(\bar{v}_{\infty,x})^{3/2} \qquad (11)$$

A value of $T_W/T_O = 0.15$ was used to agree with the average wall temperature condition of the present data.

The free molecule flow limit was calculated using the expression given by Wallace and Burke (Ref. 19)

$$M_\infty\, C_H)_{FM} = \frac{1}{(2\pi\gamma)^{1/2}} \quad \frac{a_c}{1 - (H_w/H_o)} \left[1 + \frac{\gamma - 1}{\gamma(\gamma-1)M_\infty^2}\,(1 - T_w/T_o)\right] \qquad (12)$$

Values of $a_C = 1.0$, $H_W/H_O = 0.10$, $M_\infty = 10.1$ and $T_W/T_O = 0.14$ were used to correspond to the present data obtained at the highest values of $\bar{v}_{\infty,x}$.

When the present data are compared to these two predictions, it can be seen that the local heat transfer is significantly higher than strong interaction results below $\bar{v}_{\infty,x} = 0.3$ (also see Fig. 8a), and that the free molecule value has been approached at a value of $\bar{v}_{\infty,x} \approx 0.5$. A slight overshoot above the free molecule prediction can also be inferred. The apparent attainment of the free molecule limit would correspond to a Knudsen number, λ_∞/x, of about 0.05 in the present case. Since this value is at least two orders of magnitude less than what might be expected, one would be tempted to explain this result as evidence of a strong overshoot as the leading edge is approached from downstream. However, the Mach 20 results of Vidal and Bartz (Ref. 3) indicate that this is not the case, and a constant value of C_H slightly above free molecule predictions is measured at a position far downstream of the leading edge. The very strong pressure overshoot (Refs. 12 and 13) near the leading edge is not duplicated in regard to heat transfer.

Of the theoretical predictions shown in Fig. 16, only those of Chow (Ref. 7) and Rudman and Rubin (Ref. 8) may be directly compared to the present results. The calculations of Rudman and Rubin, which were done for Mach numbers of 50, 25, and 15, were extrapolated at constant values of $\bar{v}_{\infty,x}$ to the present Mach number of 10. This

extrapolation leads to only a small difference between M_∞ = 15 and 10 being found. However, a relatively large effect of M_∞ between M_∞ = 15 and 25 was noted in Ref. 8. Quantitative comparison between data and the theory of Rudman and Rubin is excellent. The results of Chow (Ref. 7), although being qualitatively in agreement, underestimate the heat transfer by a considerable amount. Since comparison with Chow's numerical results for other parameters (such as surface pressure, density, slip, velocity, and shock angle) in Ref. 7 is excellent, the failure to predict quantitative heat-transfer rate is puzzling. The recent results of Cheng (Ref. 5) and Shorenstein and Probstein (Ref. 6) both underestimate the present heating rates. Since both of these solutions assume strong shocks ($M_\infty >> 1$), they would be expected to agree with strong interaction results in the downstream portion of the flow and the underestimation of the present results by strong interaction theory is consistent with these theories. The Mach 20 data of Vidal and Bartz (Ref. 3) are in excellent agreement with the theory of Shorenstein and Probstein. The kinetic theory approach of Huang and Hartley (Ref. 9) is in qualitative agreement with the present results although the flow conditions for which the calculations were performed are substantially different than the present experimental conditions. Huang's and Hartley's numerical results clearly indicate a nonexistence of a marked strong interaction flow regime at low supersonic Mach numbers (for which $C_H/\bar{v}_{\infty,x}^{3/2}$ is a constant in Fig. 16). This has been observed experimentally in surface pressure measurements (Refs. 13 and 20). The Monte Carlo results of Vogenitz et al. (Ref. 10) are compared to the present data in Fig. 17. Although the calculations were performed for slightly different free-stream conditions and, more importantly, a monatomic gas, the qualitative agreement with the present results is very good. A large influence of the degree of accommodation is seen in the theoretical results. The present data are inadequate to test this result experimentally since they were obtained in a diatomic gas. They have been normalized by use of Eq. (12) with a_c = 1.

A rather strong influence of Mach number in the range $10 \leqq M_\infty \leqq 20$ is suggested in Fig. 18. Some early heat-transfer data obtained in the range $8 \leqq M_\infty \leqq 11$ from Refs. 2 and 4 are compared to the present results. Although data scatter is large, qualitative agreement is good and indicates an increase of from 50 to 100 percent in the local heat-transfer coefficient over that measured in flows of much higher Mach numbers. The data are presented in the manner suggested by Shorenstein and Probstein. Calculations of $C_H)_{FM}/C_H)_{SI}$ for the flow condition of the present data are also shown.

5.2 LARGE WEDGE ANGLE DATA

A comprehensive theoretical treatment of hypersonic viscous flow over a wedge was first presented by Cheng et al. (Ref. 2) in 1961. Using a strong shock assumption with Prandtl number of unity and allowing $\gamma \rightarrow 1.0$, Cheng developed his boundary-layer displacement theory for large wedge angles. Comparison of high Mach number data in Ref. 3 gave reasonable agreement in regard to heat transfer. Data presented in Cheng's original paper at Mach numbers near 12 indicated measured heat transfer greater than predicted. These results were confirmed by the present investigation (Figs. 8b and c). Since the strong shock assumption is obviously not satisfied in the present case, no further comparison of the data was made with theories based on this premise.

For wedge angles smaller than that necessary for shock detachment to occur, the present two-dimensional problem can be directly related to the flat plate at zero angle of attack by using local inviscid flow properties calculated from perfect gas wedge theory. Redefining C_H and $\bar{v}_{\infty,x}$ yields

$$C_{H_i} = C_H \rho_\infty U_\infty / \rho_i U_i \tag{13}$$

$$\bar{v}_{i,x} = M_i \sqrt{C_i} / \sqrt{Re_{i,x}} \tag{14}$$

where the subscript i refers to the inviscid values at the edge of the boundary layer. Although this is a fictitious condition since in the merged layer no such inviscid region exists, it is consistent with the use of free-stream values in reducing zero angle-of-attack data. The present data obtained at α = 10 and 20 deg were reduced using Eqs. (13) and (14) and are shown in Fig. 19. The data shown in Fig. 16 are also included for comparison using $C_{H_i} = C_H$ and $\bar{v}_{i,x} = \bar{v}_{\infty,x}$. The effect of this correlation of the data is to increase the rarefaction range of the data. Local inviscid Mach number, M_i, was about 4.2 at α = 10 deg and 6.5 at α = 20 deg. Although the data shown in Fig. 19 at α = 0, 10, and 20 deg appear at first to agree, there is actually a distinct Mach number effect between the three sets of data. The Mach 4.2 data are somewhat above the Mach 6.5 data which in turn are in reasonable agreement with the Mach 10 data. In addition, weak interaction and free molecule theory predict a considerable shift in C_{H_i} for a given value of $\bar{v}_{i,x}$. The $M_i \approx 4.2$ data appear to be fairing directly into the free molecule solution with no region of strong interaction ($C_{H_i} / \bar{v}_{i,x}^{3/2}$ = constant) being present. The Mach 10 data appear to have a small range of constant $C_{H)_i} / \bar{v}_{i,x}^{3/2}$ although sufficient data are lacking to measure the extent of the plateau. The $M_i \approx 6.5$ also are inadequate in this respect.

SECTION VI
CONCLUDING COMMENTS

The feasibility of utilizing phase-change temperature-sensitive paint in place of conventional heat-transfer instrumentation in low-density flows has been demonstrated. Investigations which involve small, complex models for which heat-transfer instrumentation would be very difficult would be greatly facilitated by this technique. The main restrictions include the necessity of using a low conductivity material for which physical and thermal properties are known and approximating a step heat input to a flow where the heat-transfer coefficient, h, is a constant. The selection of the proper material and paint depends on knowledge of the expected range of local heat-transfer rate. Heat transfer by conduction or radiation into the test material must be eliminated by proper model construction.

Results of the present measurements of local heat-transfer rates to a sharp-leading-edge flat plate can be summarized as follows:

1. In the range $4 \leqq M_i \leqq 10$ and $0.06 \leqq \bar{v}_{i,x} \leqq 0.8$, there is no distinct region of strong interaction in which $C_{H_i} \Big/ \bar{v}_{i,x}^{3/2}$ = constant.
2. Strong interaction theory underestimates the local heat-transfer rate in the Mach number range investigated.
3. Free molecular flow values of C_H are approached at Knudsen numbers much smaller than might be expected but free molecule theory underestimates the heat transfer near the leading edge in the present case.
4. A strong Mach number influence between M_∞ = 10 and 20 data is observed when comparison with published data is made.
5. The present results are predicted both quantitatively and qualitatively by the theory of Rudman and Rubin (Ref. 8) and qualitatively by several other theoretical studies.

The necessity of being able to measure local heat-transfer rates in the present flow regime will become greater in the design of future manned and unmanned slender lifting bodies. The interpretation of measured surface pressures in this flow regime has also been shown to be dependent on accurate knowledge of the local heat transfer (Ref. 21). An example of this is the surface pressure measurements reported in Ref. 13. When those measurements were made, the only applicable heat-transfer data available were the M_∞ = 20 data contained in Ref. 3.

The present measurements indicate that actual heat-transfer rates as much as two times greater should have been used in the data analysis. Although the maximum error in the published wall pressure data in Ref. 13 is not large, amounting to only 8 percent with the data being corrected to a higher wall pressure level, the influence of an inaccurate estimation of heating rate in certain cases could be quite large.

REFERENCES

1. Gregorek, G. M. and Lee, J. D. "Heat Transfer Measurements in Hypersonic Low-Density Flows by Thin Skin Techniques and Phase-Change Coatings." AIAA Paper No. 68-373, April 1968.
2. Cheng, H. K., Hall, J. Gordon, Golian, T. C. and Hertzberg, A. "Boundary-Layer Displacement and Leading-Edge Bluntness Effects in High-Temperature Hypersonic Flow." J. Aeronautical Sciences, Vol. 28, No. 5, May 1961.
3. Vidal, Robert J. and Bartz, John A. "Surface Measurements on Sharp Flat Plates and Wedges in Low-Density Hypersonic Flow." CAL No. AF-2041-A-2, February 1968.
4. Nagamatsu, H. T., Weil, J. A. and Sheer, R. E., Jr. "Heat Transfer to Flat Plate in High Temperature Rarefied Ultra-high Mach Number Flow." ARS Journal, April 1962, pp. 533-541.
5. Cheng, H. K., Chen, S. Y., Mobley, R., and Huber, C. "On the Hypersonic Leading Edge Problem in the Merged-Layer Regime." Sixth Rarefied Gas Dynamics Meeting, Boston, Massachusetts, July 1968.
6. Shorenstein, M. L. and Probstein, R. F. "The Hypersonic Leading-Edge Problem." AIAA Journal, Vol. 6, No. 10, October 1968.
7. Chow, W. L. "Hypersonic Rarefied Flow Past the Sharp Leading Edge of a Flat Plate." AIAA Journal, September 1967.
8. Rudman, S. and Rubin, S. G. "Hypersonic Viscous Flow over Slender Bodies with Sharp Leading Edges." AIAA Journal, Vol. 6, No. 10, October 1968.
9. Huang, A. B. and Hartley, D. L. "Kinetic Theory of the Sharp Leading Edge Problem. I. Supersonic Flow." Presented at the 18th International Astronautical Congress, Belgrade, Yugoslavia, September 1967.

10. Vogenitz, F. W., Broadwell, J. E., and Bird, G. A. "Leading Edge Flow by the Monte Carlo Direct Simulation Technique." AIAA Paper No. 69-141, January 1969.

11. Hayes, Wallace D. and Probstein, Ronald F. Hypersonic Flow Theory, Applied Mathematics and Mechanics, Vol. 5, Academic Press, New York, 1959.

12. McCrosky, W. J. "An Experimental Model for the Sharp Leading Edge Problem in Rarefied Hypersonic Flow." Report 771, March 1966, Dept. of Aero and Mech Sciences, Princeton Univ., Princeton, New Jersey. Also see AIAA Journal, Vol. 4, No. 9, September 1966, and ARL 66-0101, 1966.

13. Becker, M. and Boylan, D. E. "Flow Field and Surface Pressure Measurements in the Fully Merged and Transition Flow Regimes on a Cooled Sharp Flat Plate." AEDC-TR-66-111 (AD638804), September 1966. Also see Rarefied Gas Dynamics, 5th Symposium, Vol. 11, Edited by C. L. Brundin, Academic Press, New York, 1967, pp. 993-1014.

14. Harbour, P. J. and Lewis, J. H. "Preliminary Measurements of the Hypersonic Rarefied Flow Field on a Sharp Flat Plate Using an Electron Beam Probe." Rarefied Gas Dynamics 5th Symposium, Vol. 11, Academic Press, New York, 1967, pp. 1031-1046.

15. Potter, J. L., Kinslow, M., Arney, G. D., Jr., and Bailey, A. B. "Initial Results from a Low-Density Hypervelocity Wind Tunnel." Progress in Astronautics and Rocketry, Ed. by F. R. Riddell, Academic Press, New York, 1962, pp. 599-624.

16. Potter, J. L. and Carden, W. H. "Design of Axisymmetric Contoured Nozzles for Laminar Hypersonic Flow." AIAA Paper No. 68-372, April 1968. Also see Journal of Spacecraft and Rockets, Vol. 5, No. 9, September 1968, pp. 1095-1100.

17. Schneider, P. J. Conduction Heat Transfer, Addison Wesley Publishing Company, Inc., Reading, Massachusetts, 1957, p. 263.

18. Gardon, Robert. "An Instrument for the Direct Measurement of Intense Thermal Radiation." The Review of Scientific Instruments, Vol. 24, No. 5, May 1953.

19. Wallace, J. E. and Burke, A. F. "An Experimental Study of Surface and Flow Field Effects in Hypersonic Low Density Flow over a Flat Plate." Rarefied Gas Dynamics, Supplement 3, Vol. 1, Fourth Symposium, Academic Press, 1965.

20. Metcalf, S. C., Lillicrap, D. C. and Berry, C. J. "A Study of the Effect of Surface Temperature on the Shock Layer Development over Sharp-Edged Shapes in Low-Reynolds Number High-Speed Flow." Sixth Rarefied Gas Dynamics Meeting, Boston, Massachusetts, July 1968.

21. Kinslow, Max and Arney, George D., Jr. "Thermo-Molecular Pressure Effects in Tubes and at Orifices." AGARDograph 119, August 1967. Also presented at Sixth Rarefied Gas Dynamics Meeting, Boston, Massachusetts, July 1968.

APPENDIXES

I. ILLUSTRATIONS

II. TABLES

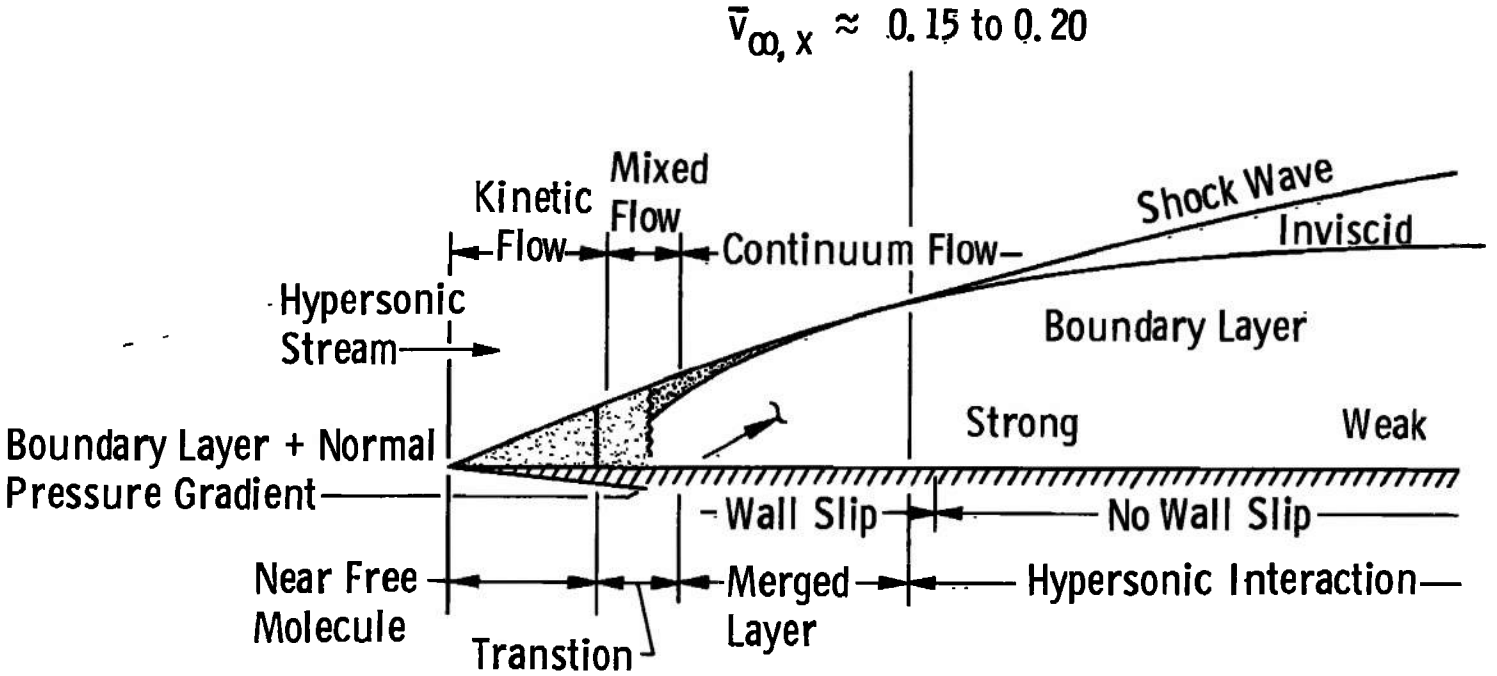

Fig. 1 Hypersonic Rarefied Flow Past a Semi-Infinite Sharp-Leading-Edge Flat Plate

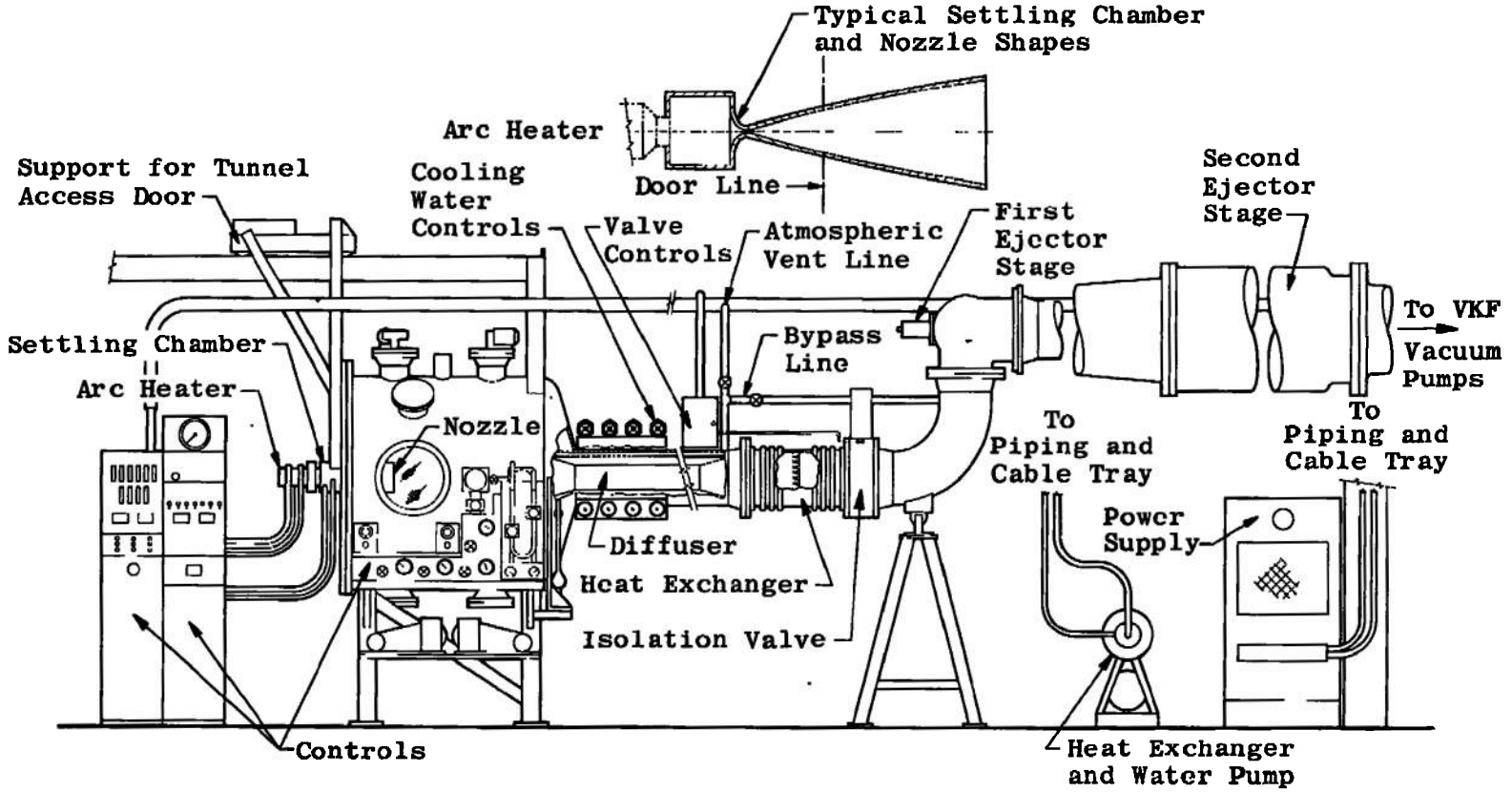

Fig. 2 Elevation View of Tunnel L

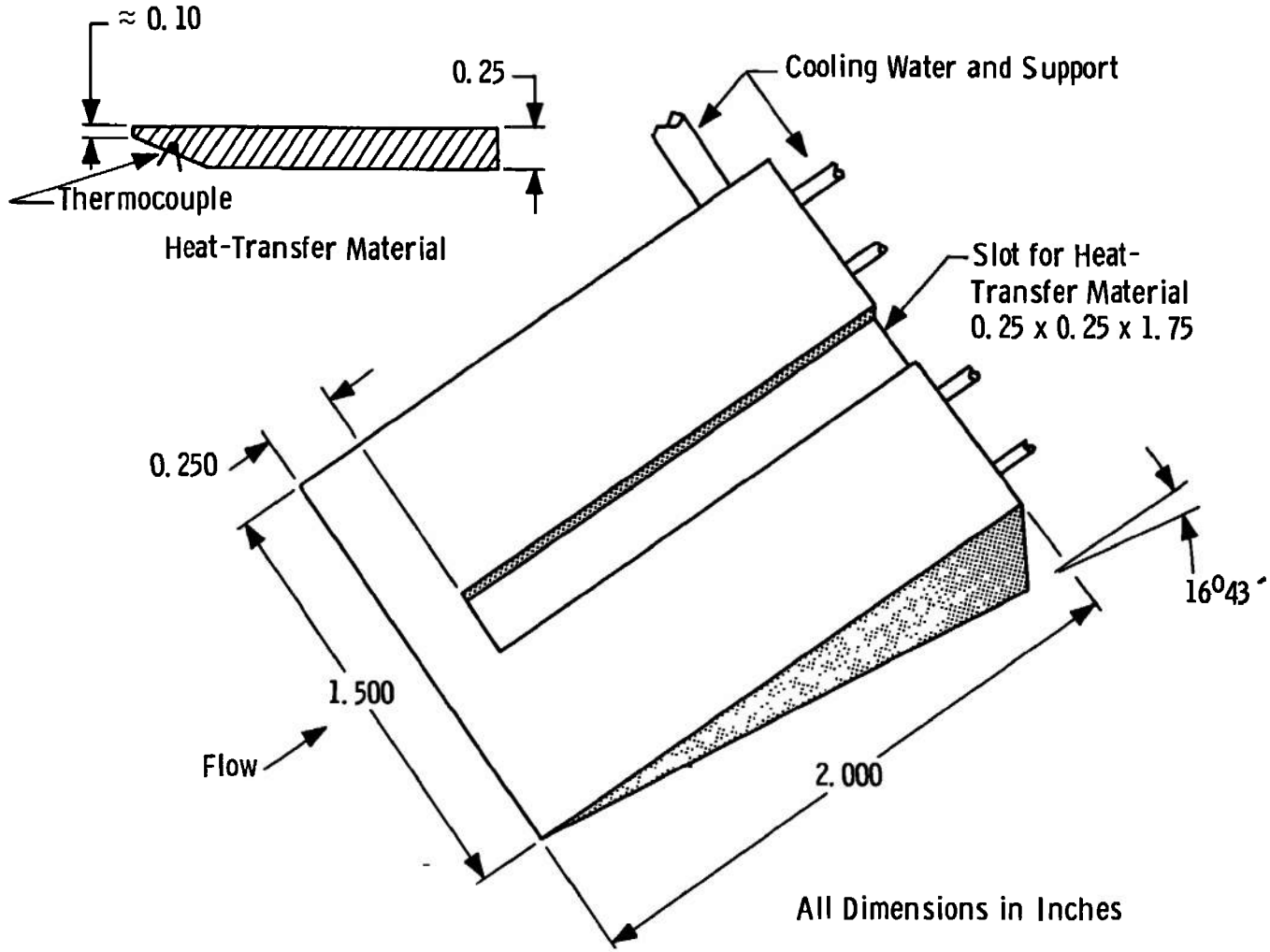

a. Model A - Phase-Change Paint Model

Fig. 3 Sketch of Flat Plate Models

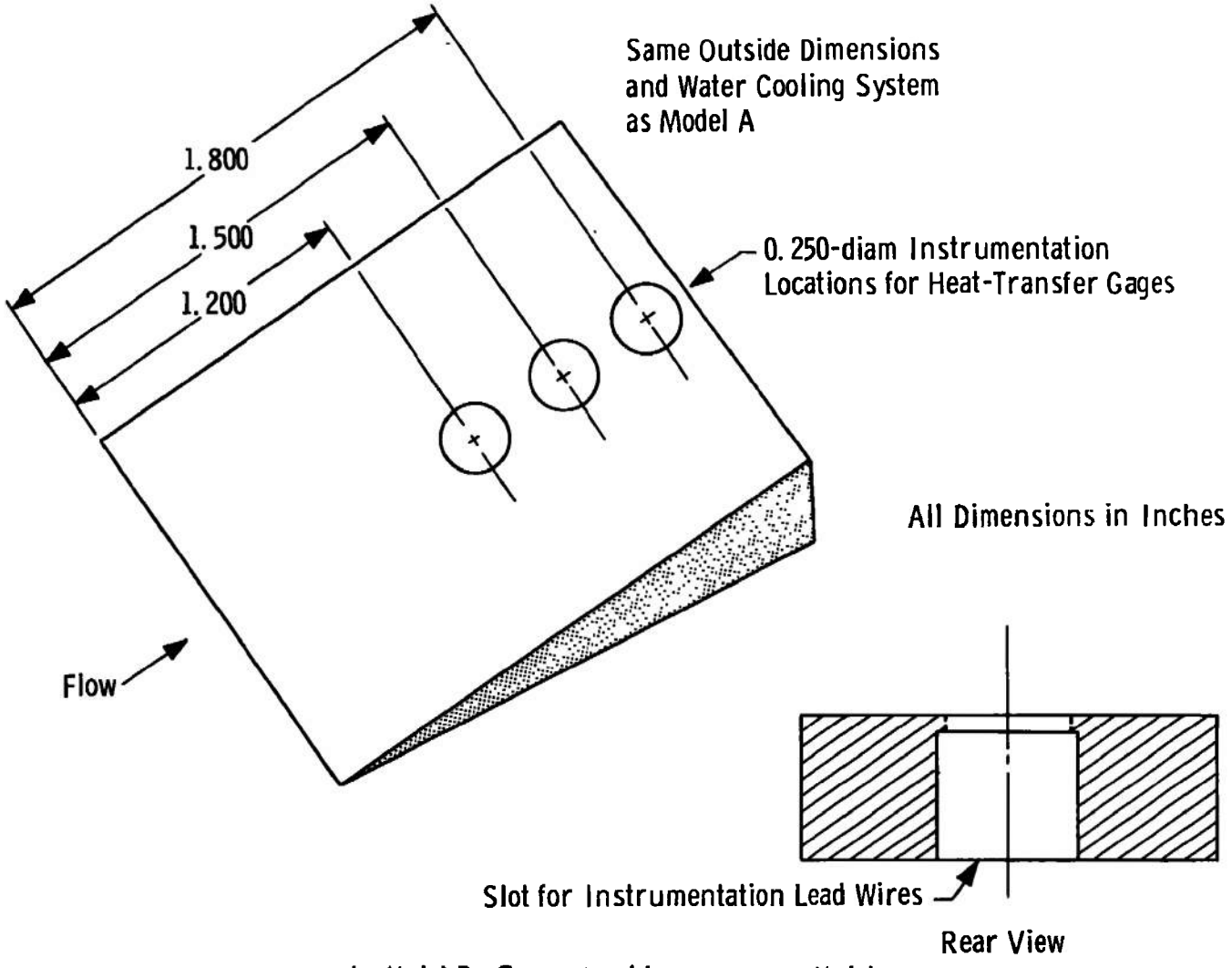

b. Model B - Conventional Instrumentation Model

Fig. 3 Concluded

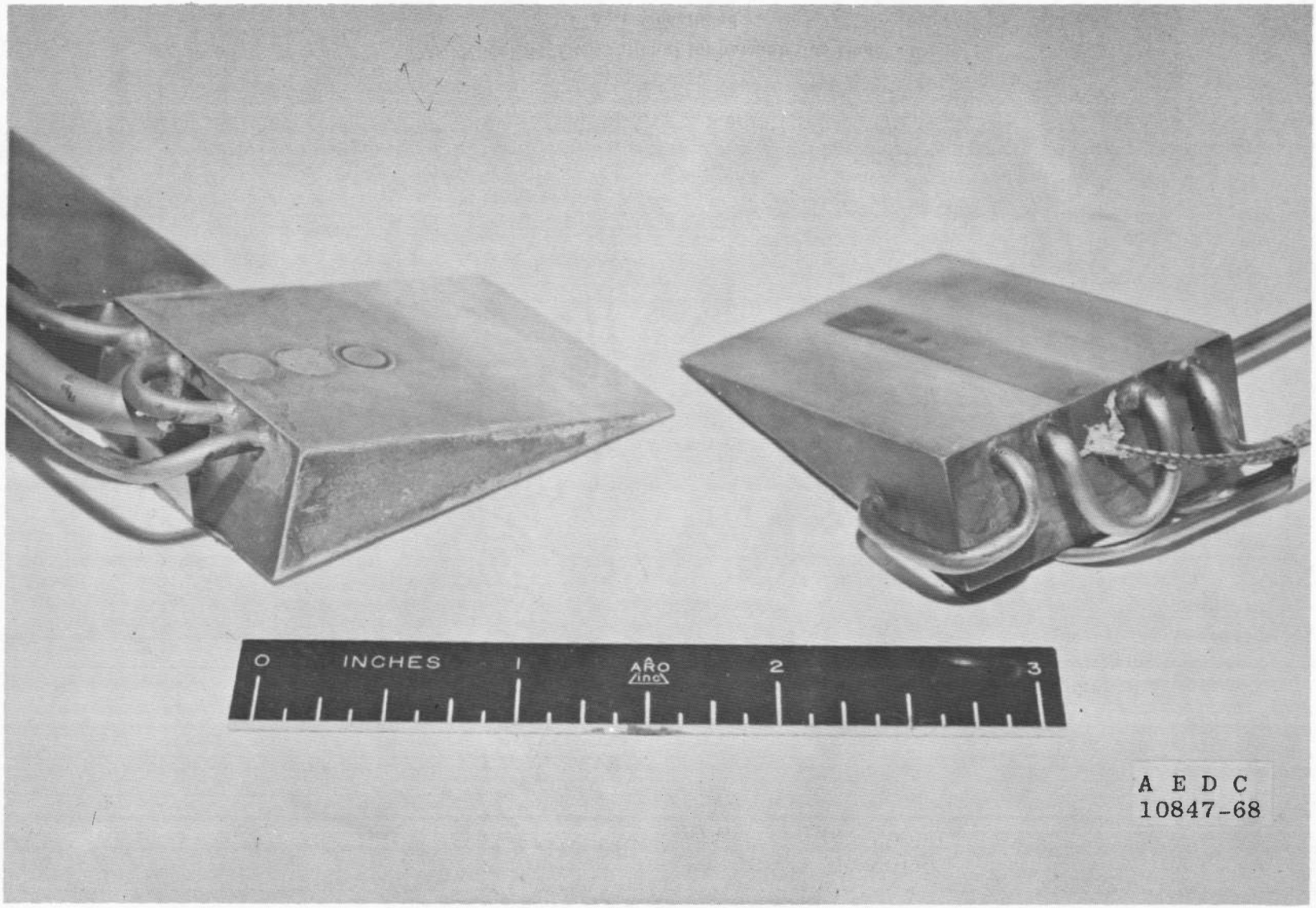

Fig. 4 Photograph of Flat Plate Model

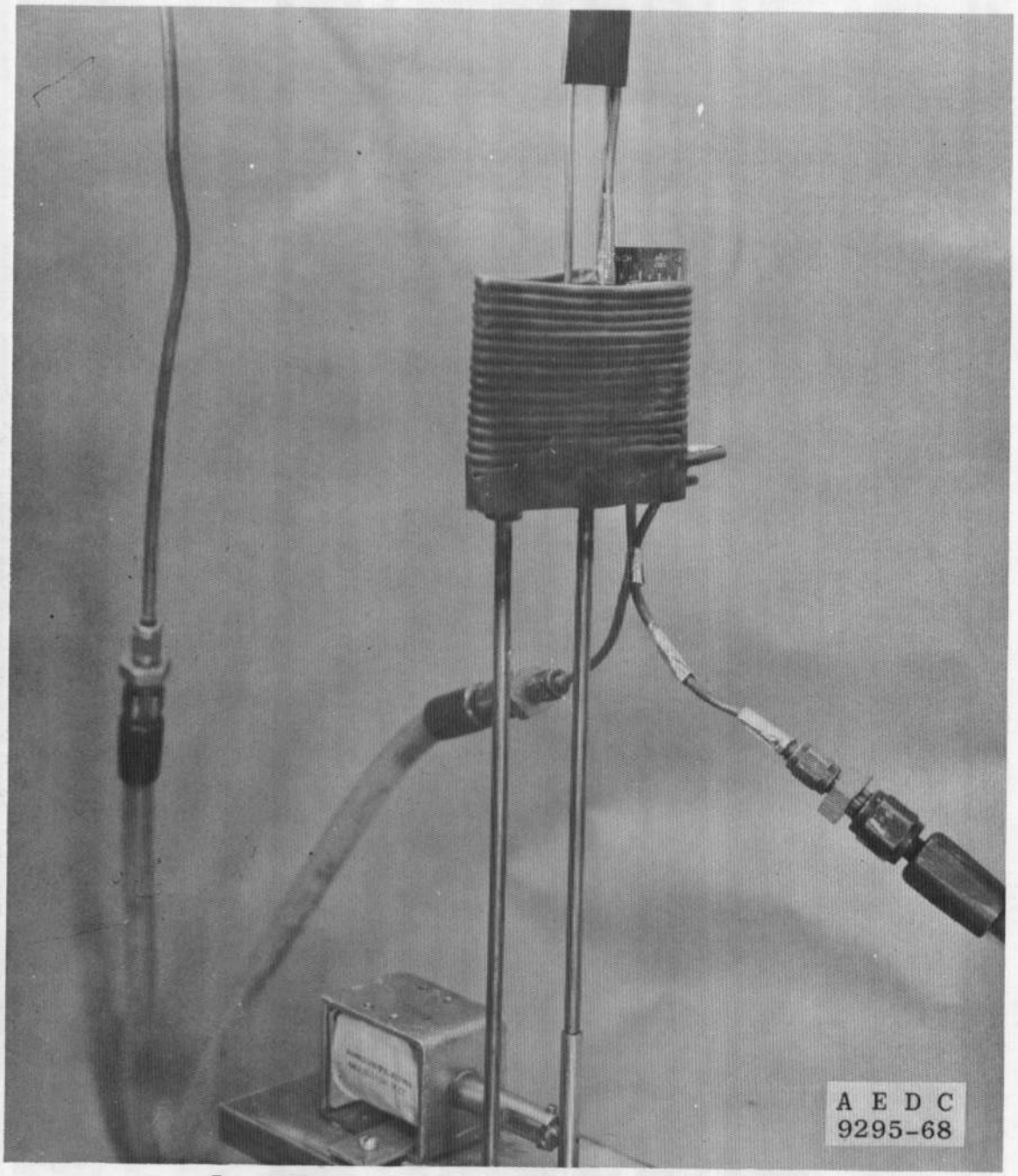

Fig. 5 Photograph of Cooling Shoe In Place around Model

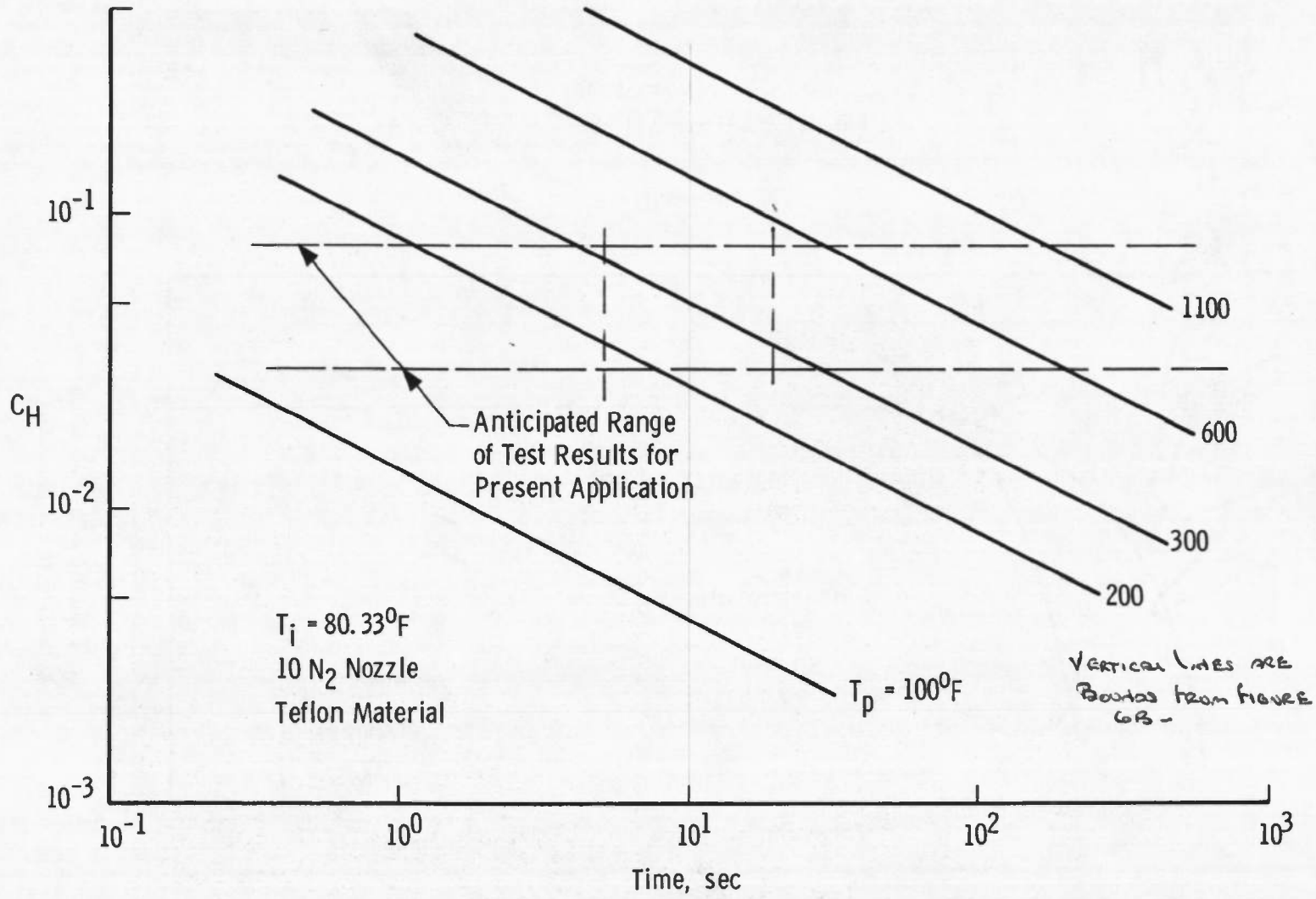

a. Evaluated at Model Surface

Fig. 6 Graphical Solution of the One-Dimensional Heat-Transfer Equation

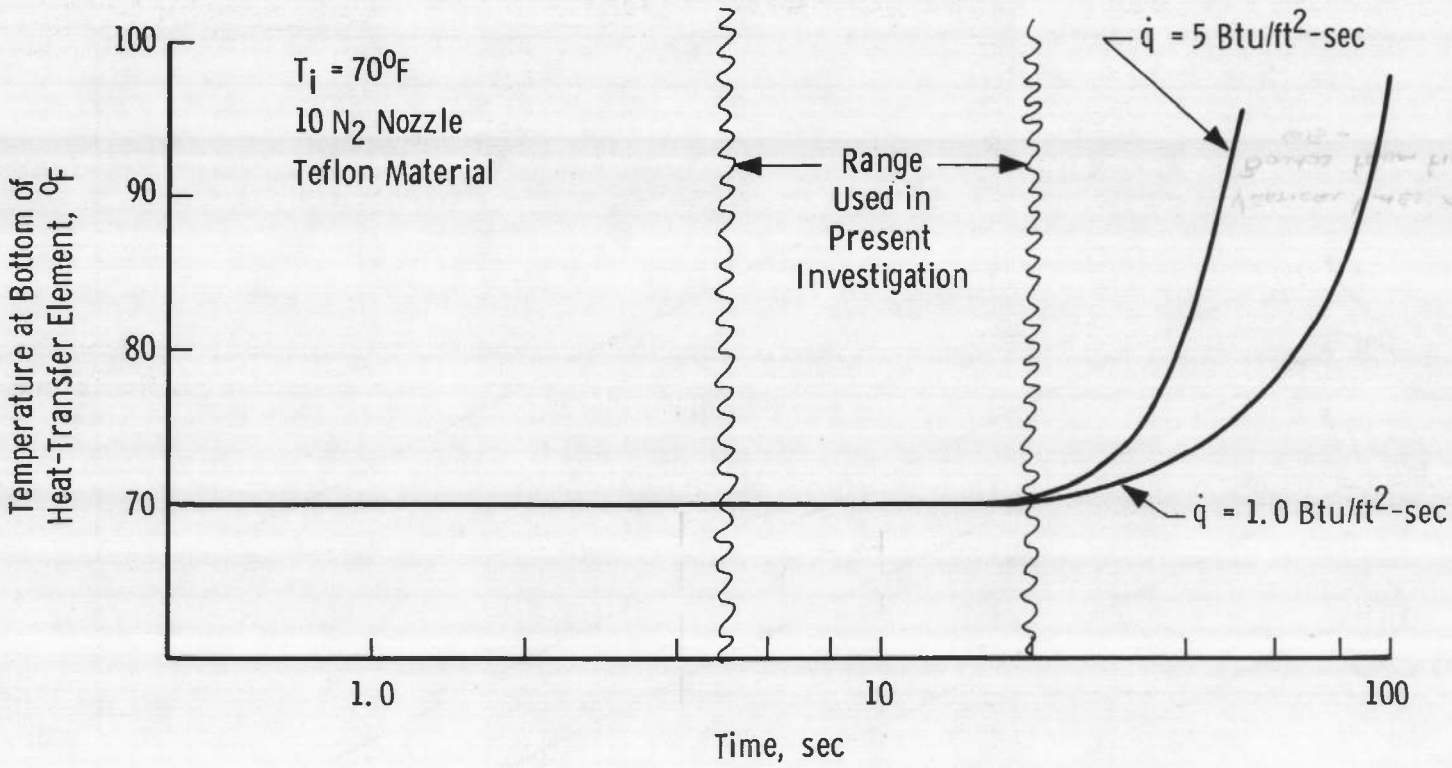

b. Evaluated at Bottom of the Heat-Transfer Material

Fig. 6 Concluded

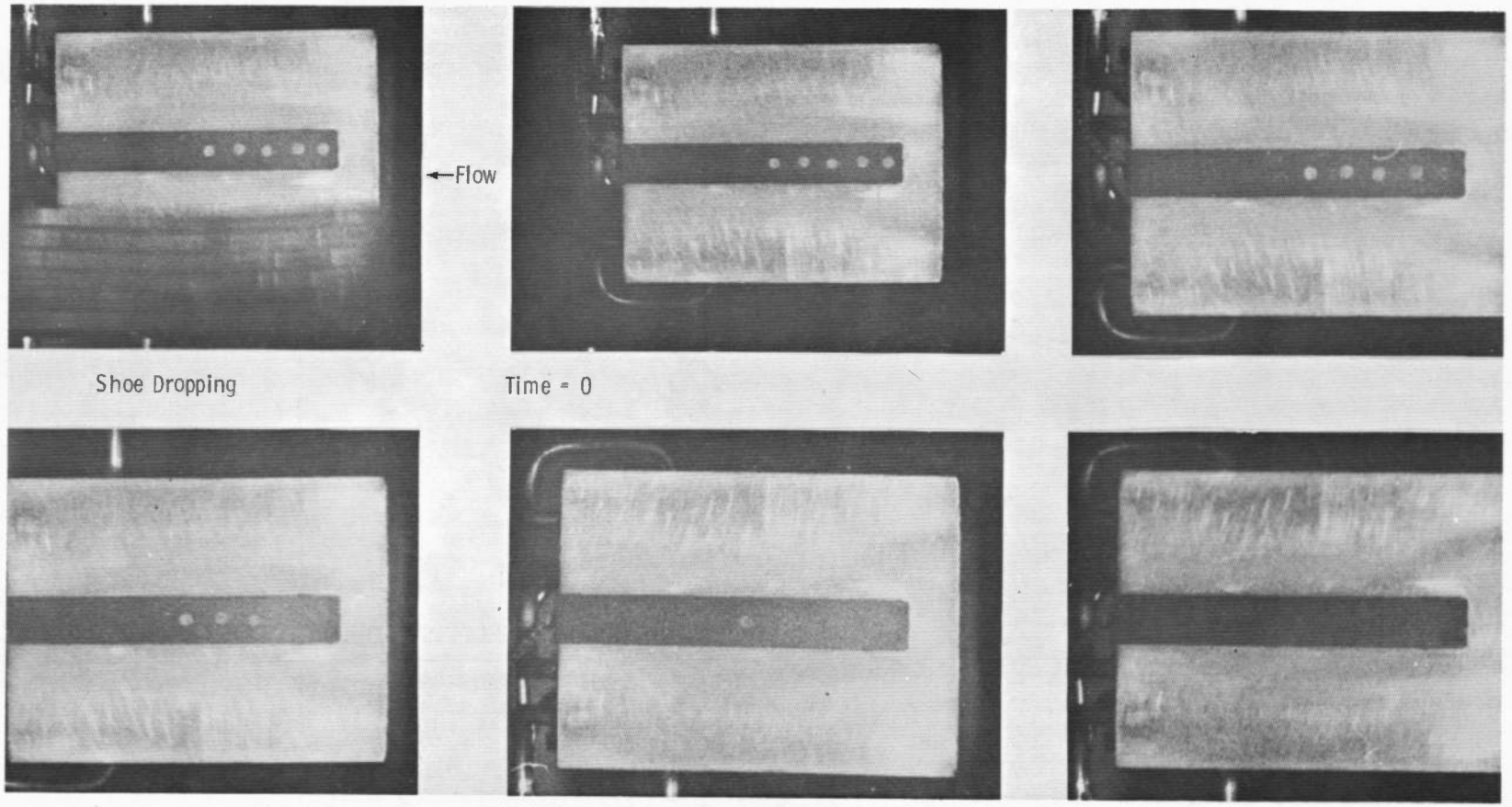

Fig. 7 Partial Photographic Record of Typical Run

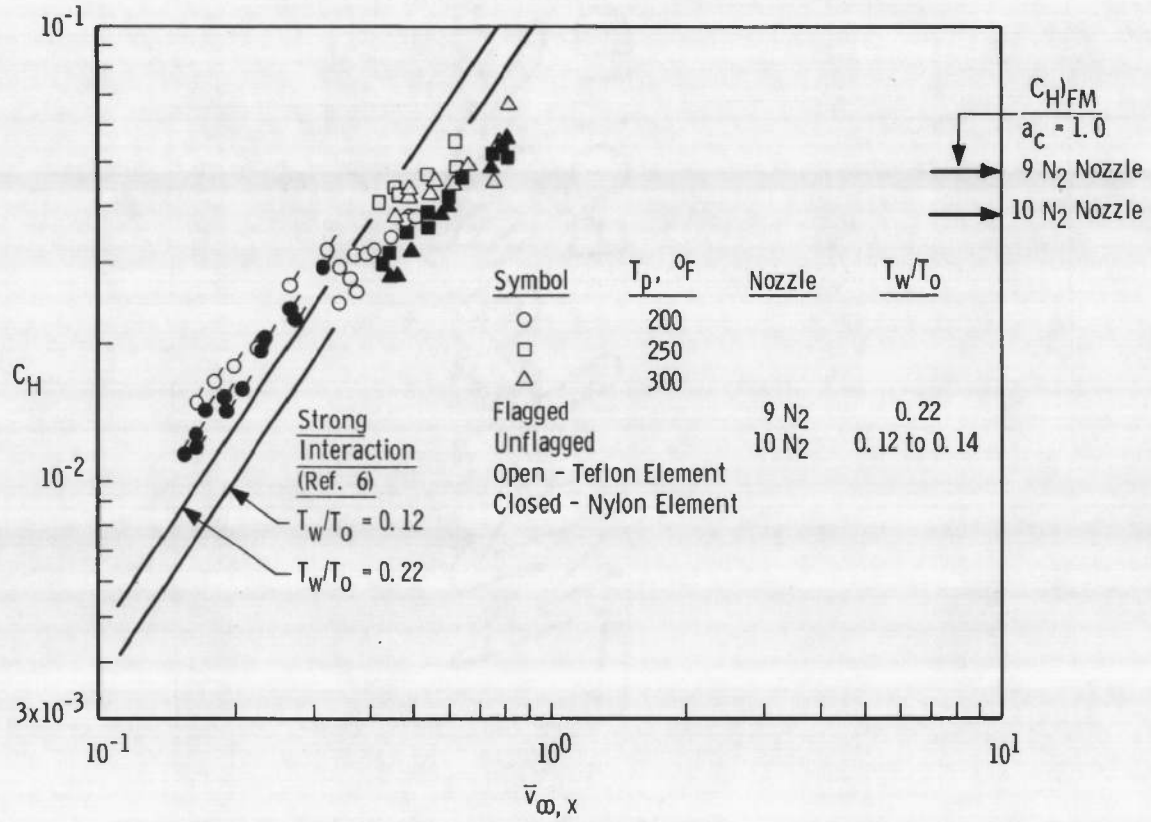

a. α = 0 deg

Fig. 8 Summary of Heat-Transfer Data Obtained from Phase-Change Paint

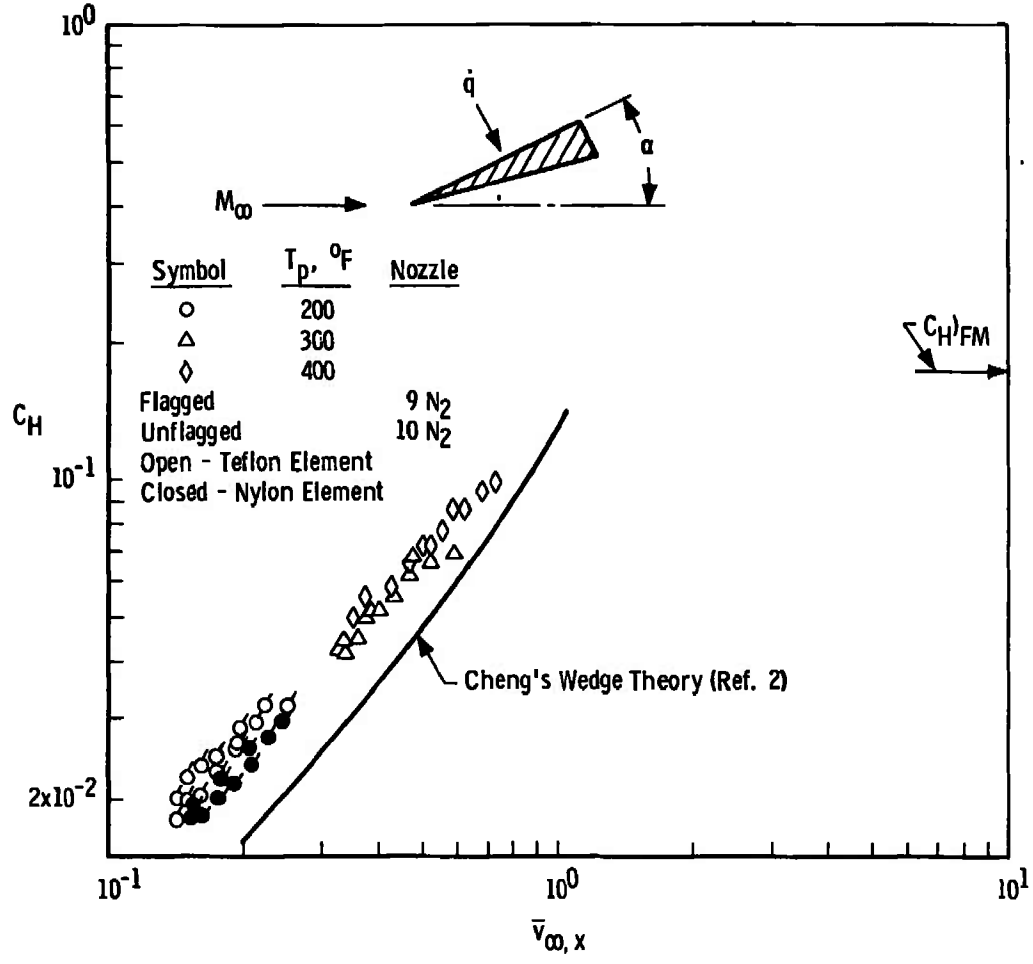

b. α = 10 deg

Fig. 8 Continued

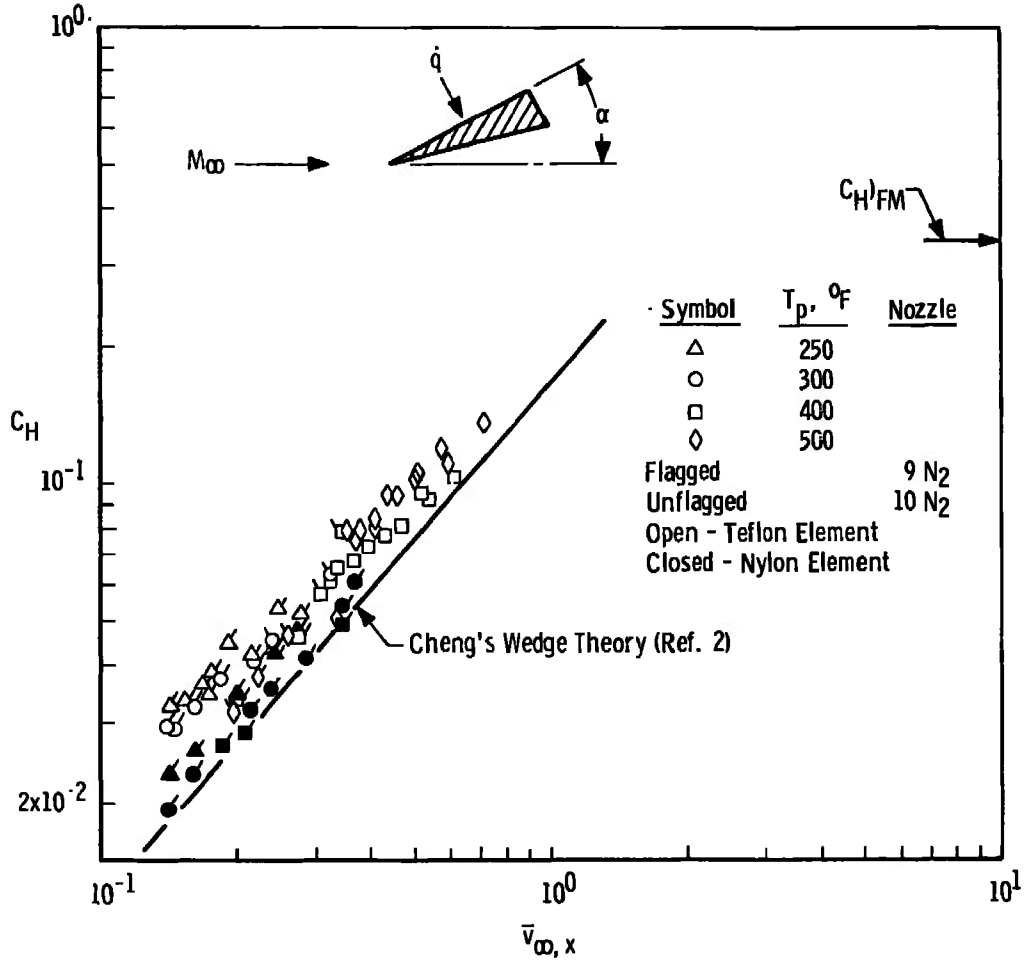

c. α = 20 deg

Fig. 8 Concluded

Sym	Nozzle	Gage
○	10 N_2	Slug Calorimeter
◔	10 N_2	Thin-Film RT
●	9 N_2	Slug Calorimeter
◕	9 N_2	Thin-Film RT

No Variation with x Could Be Observed

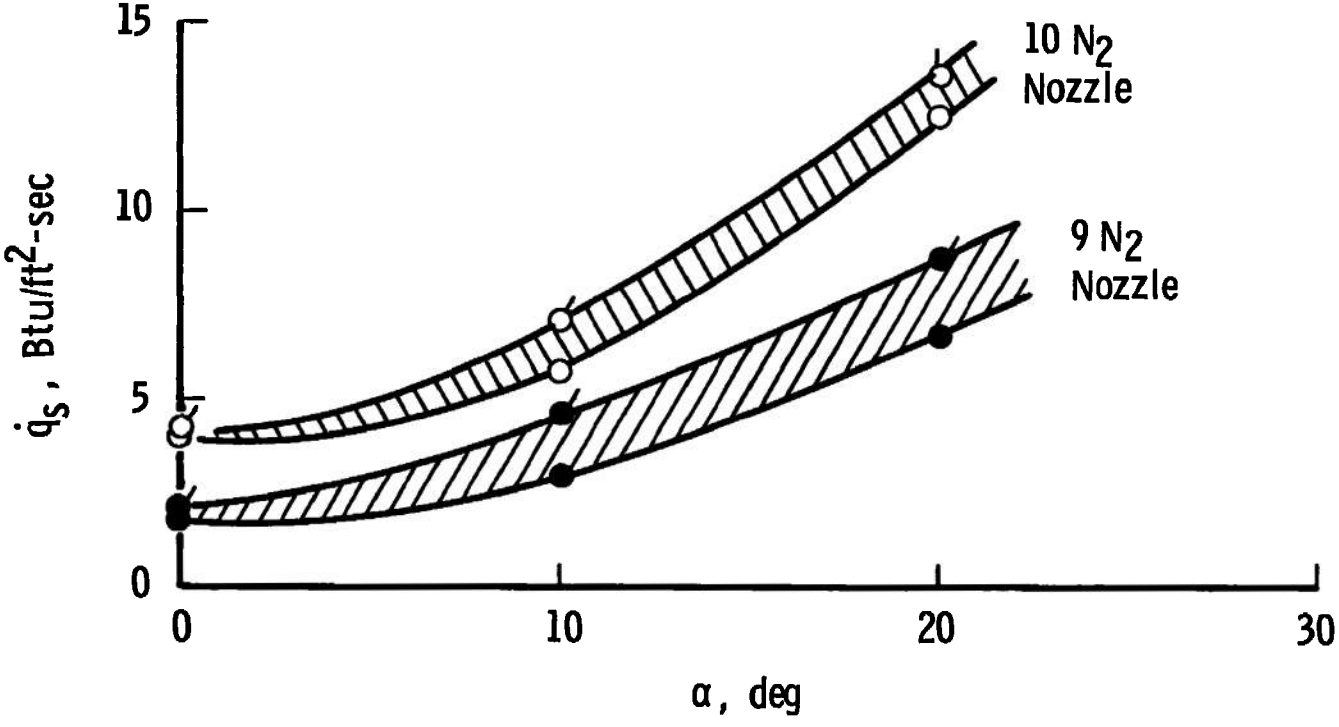

Fig. 9 Measured Heat-Transfer Rate during Flow Establishment

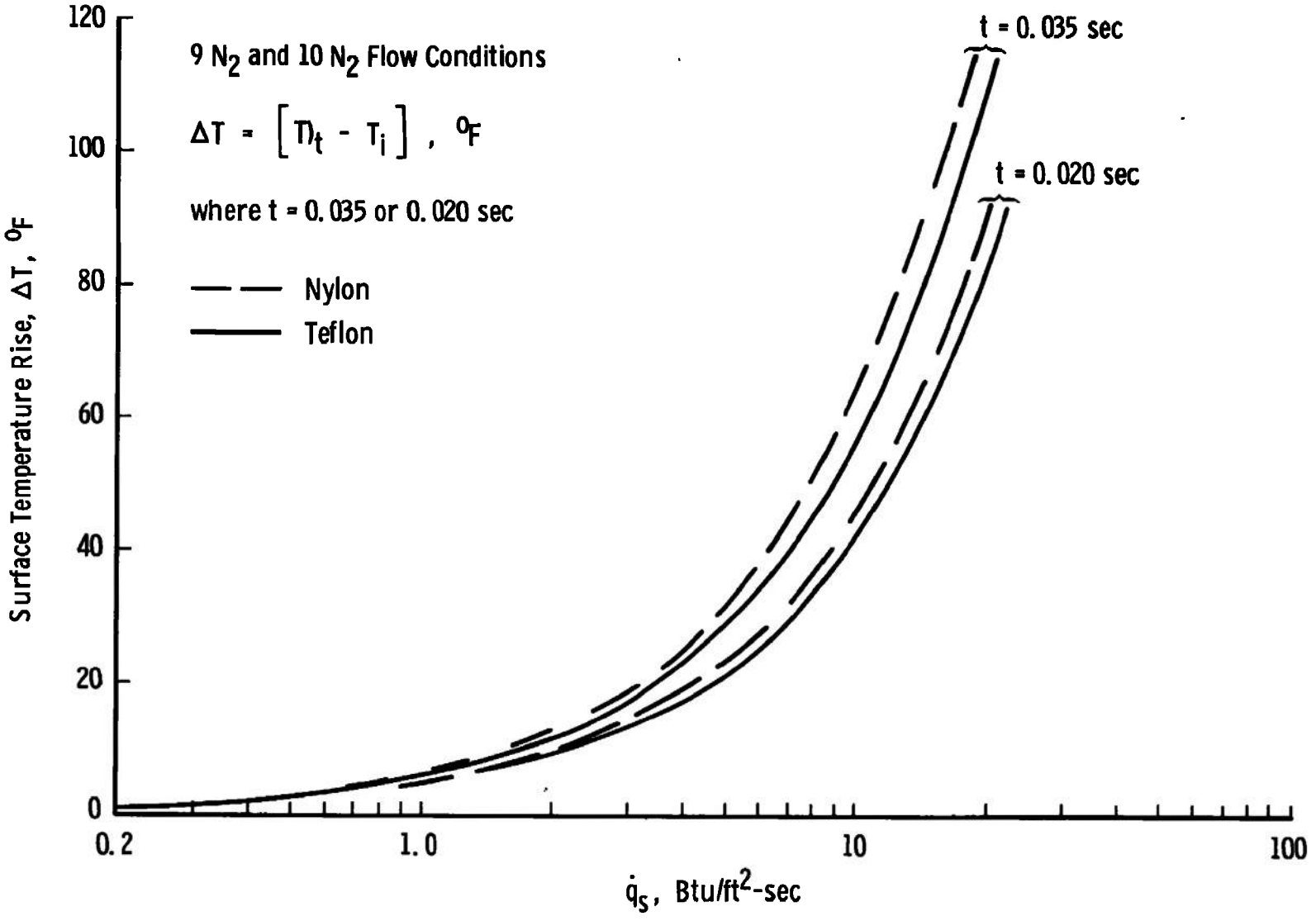

Fig. 10 Effect of Nozzle Starting Shock System on Model Surface Temperature

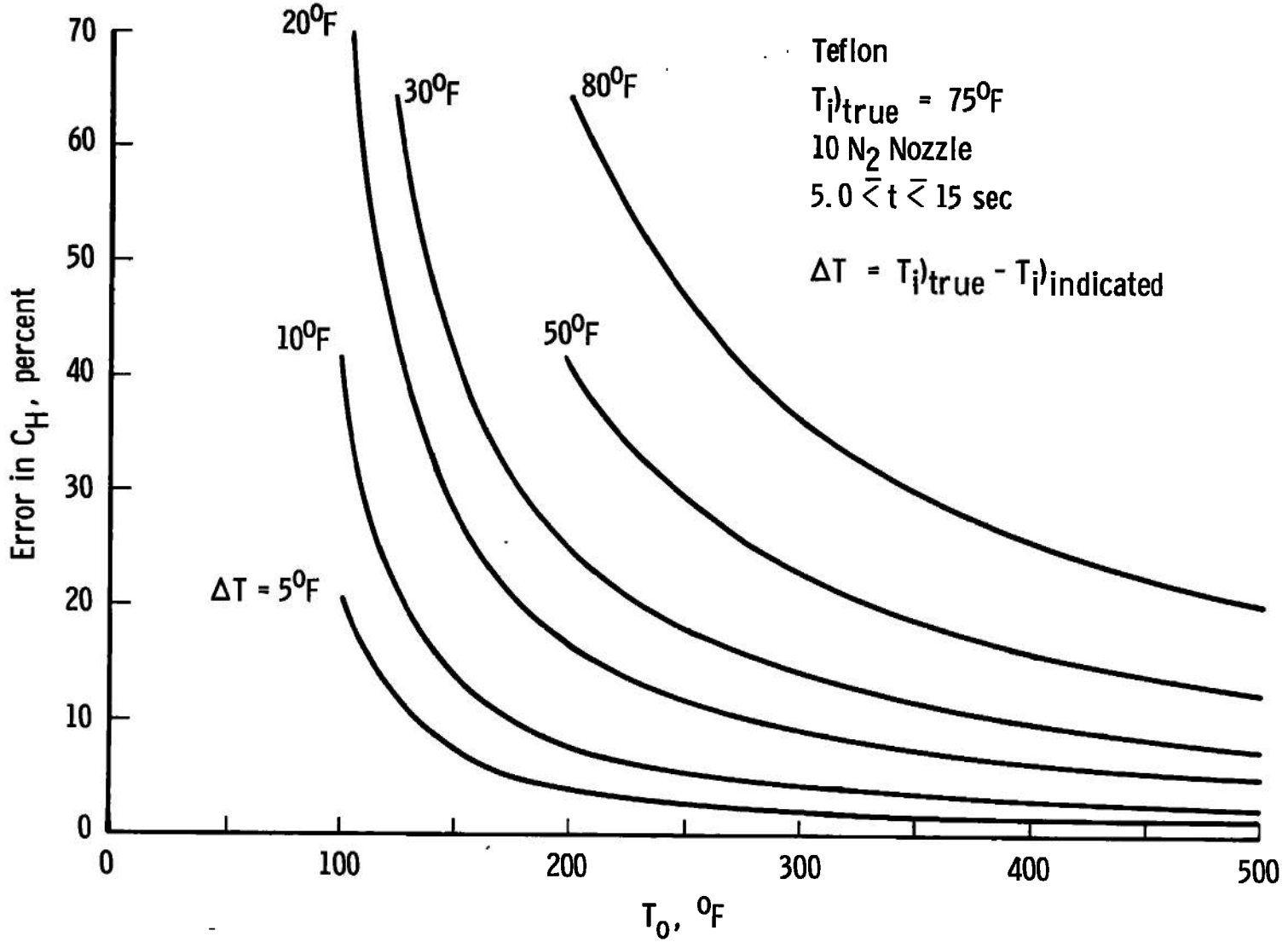

Fig. 11 Effect of Error in Initial Temperature

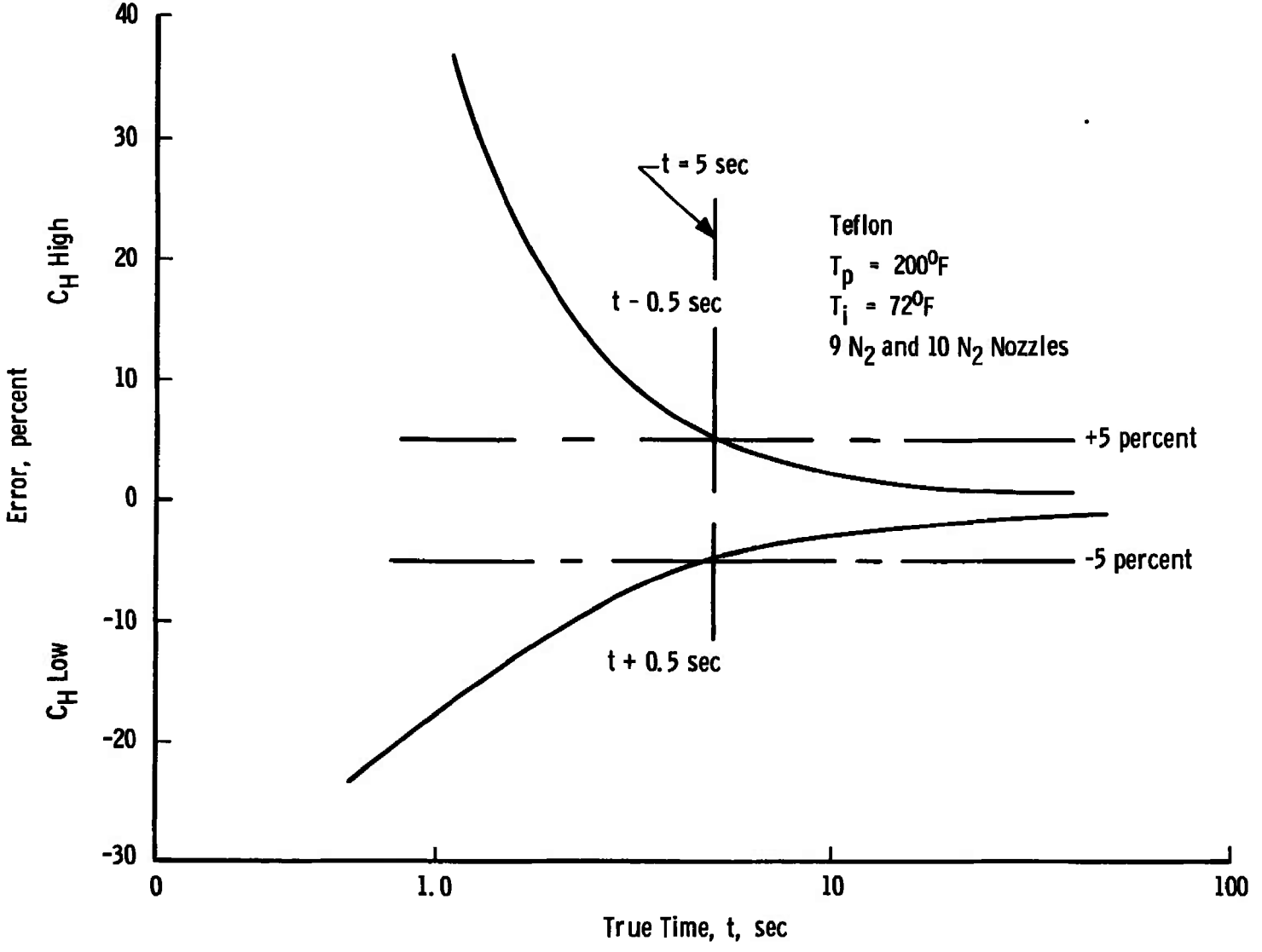

Fig. 12 Effect of Error in Measurement of Phase-Change Time

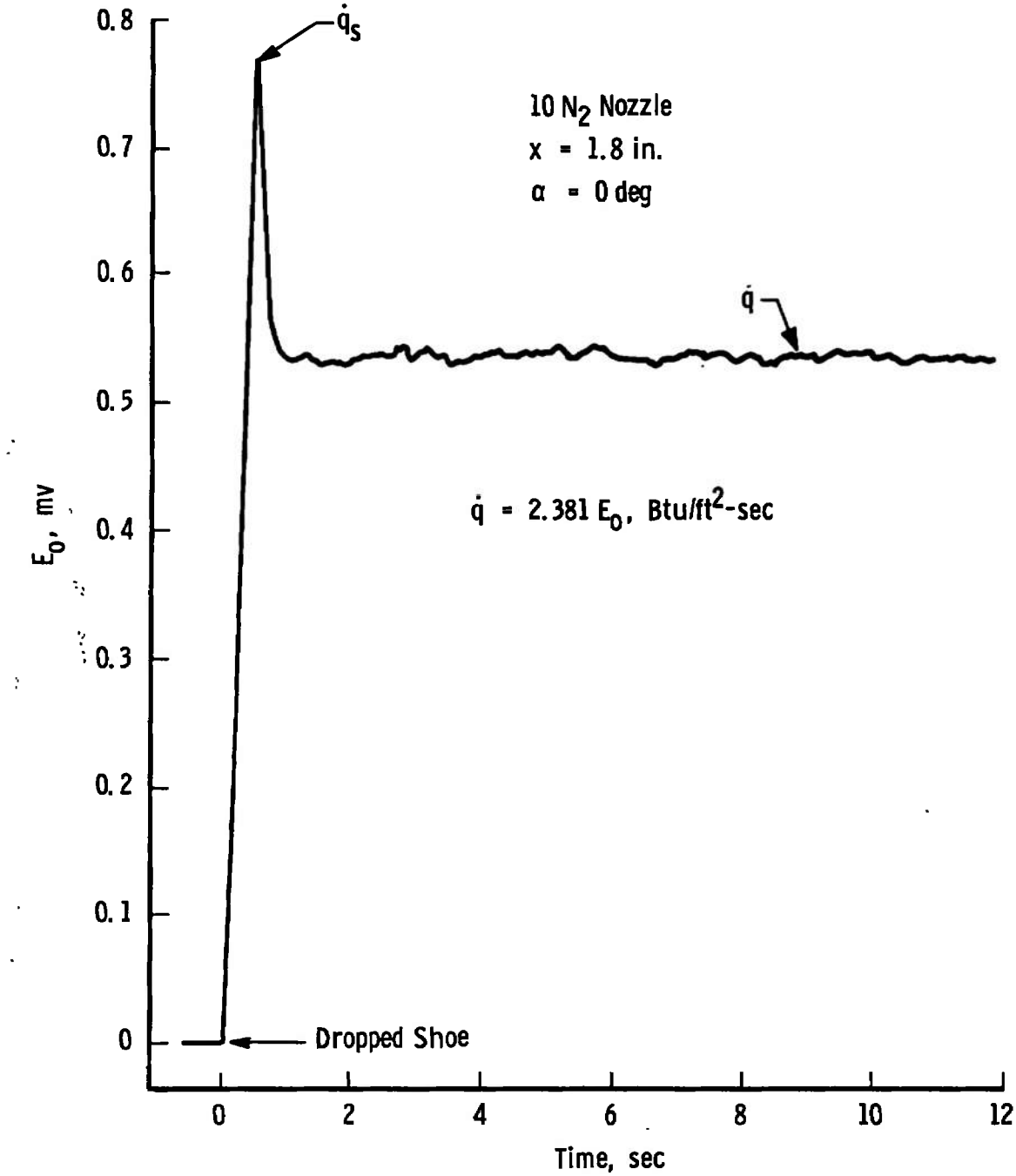

Fig. 13 Gardon Gage Output Trace

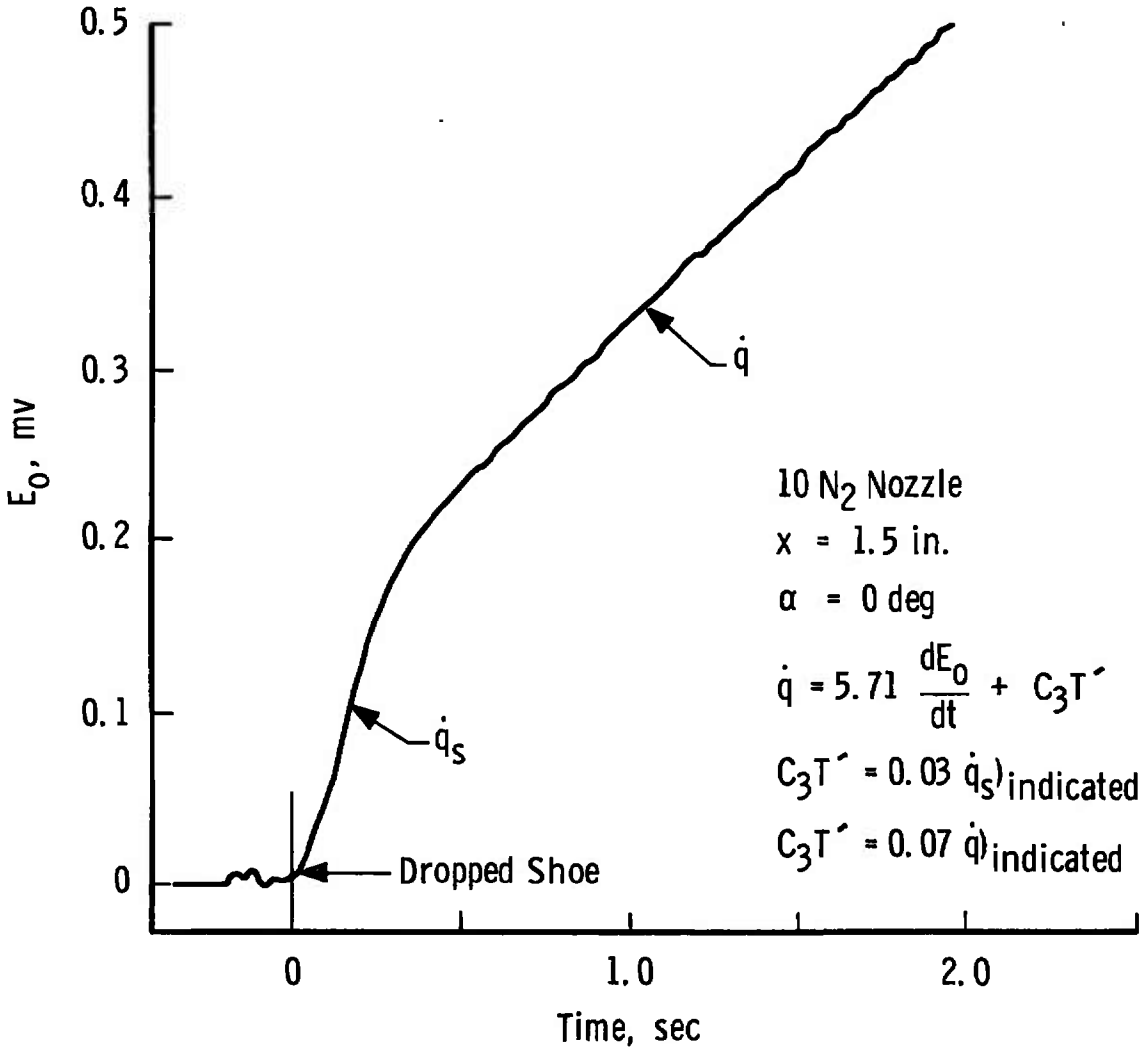

Fig. 14 Slug Calorimeter Output Trace

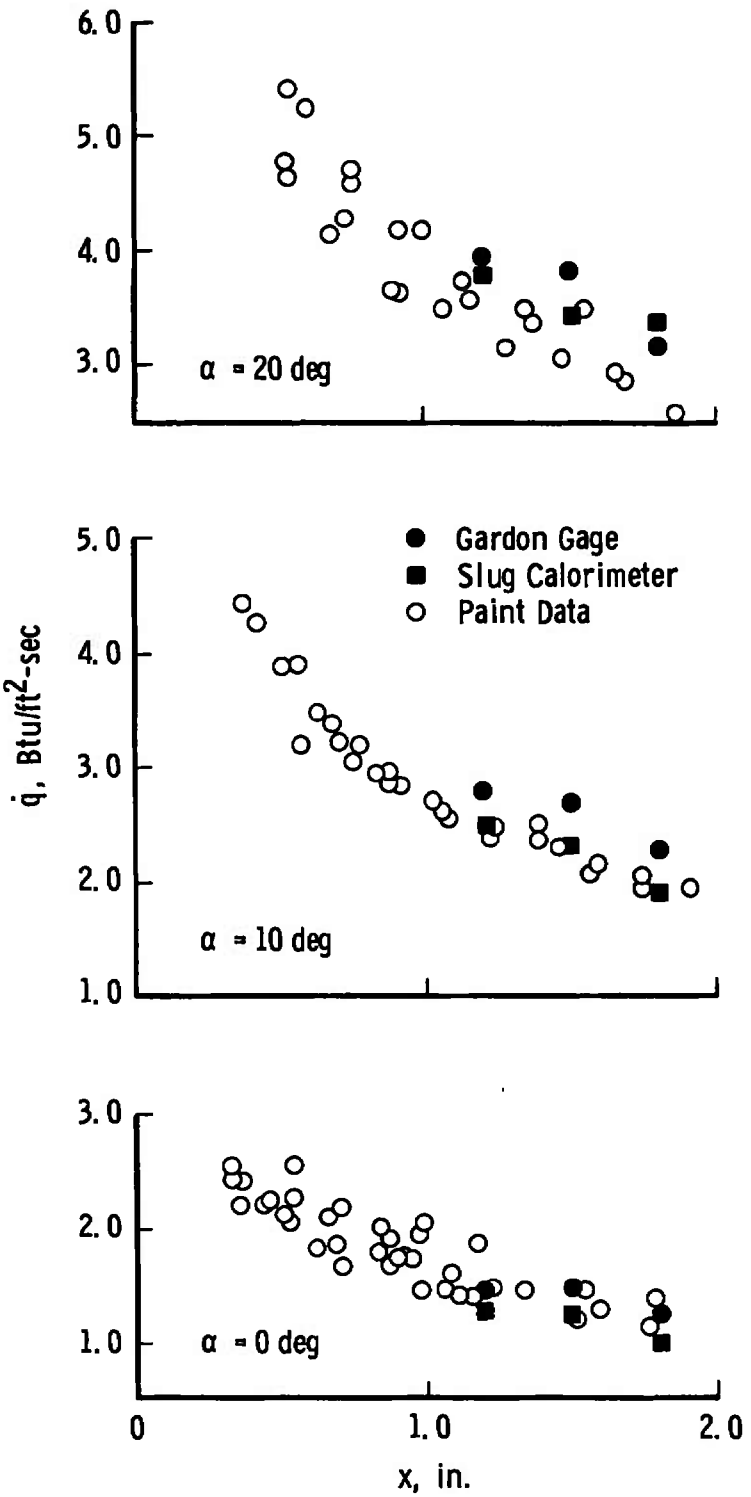

a. 10 N_2 Nozzle

Fig. 15 Comparison of Conventional Heat-Transfer Measurements to Phase-Change Paint Data

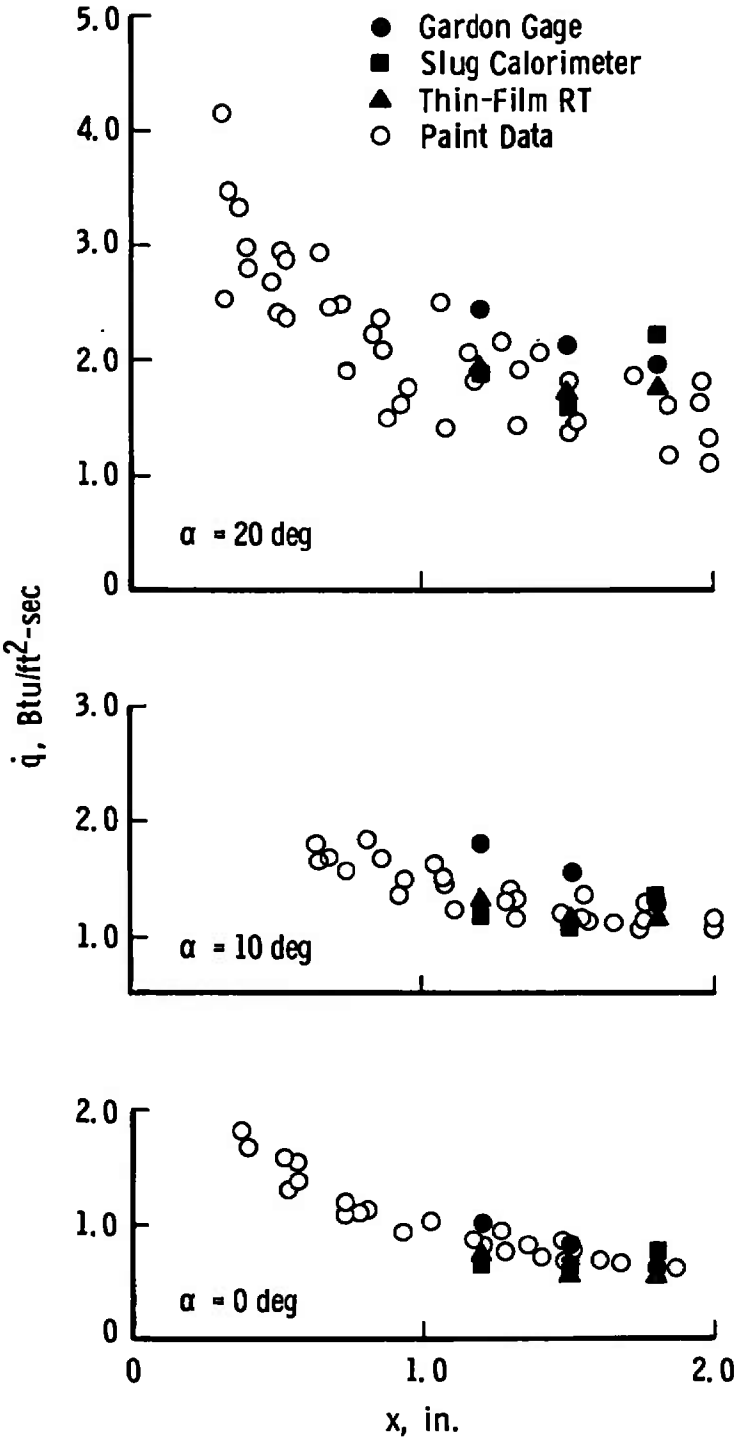

b. 9 N_2 Nozzle

Fig. 15 Concluded

Curve	Reference	M_∞	T_w/T_0	Comments
a	5	24.5	≈0.10	$c_\infty = 1.15$
b	6	>>1.0	0.15	
c	7	10	0.12	
d	8	10	0.15	Extrapolation of Ref. 8
e	8	15	0.15	
f	9	1.5	≈0.70	
g	Strong. Interaction	>>1.0	0.15	
h	Free Molecule Flow	10.1	-	$H_w/H_0 = 0.10$ $a_c = 1.0$

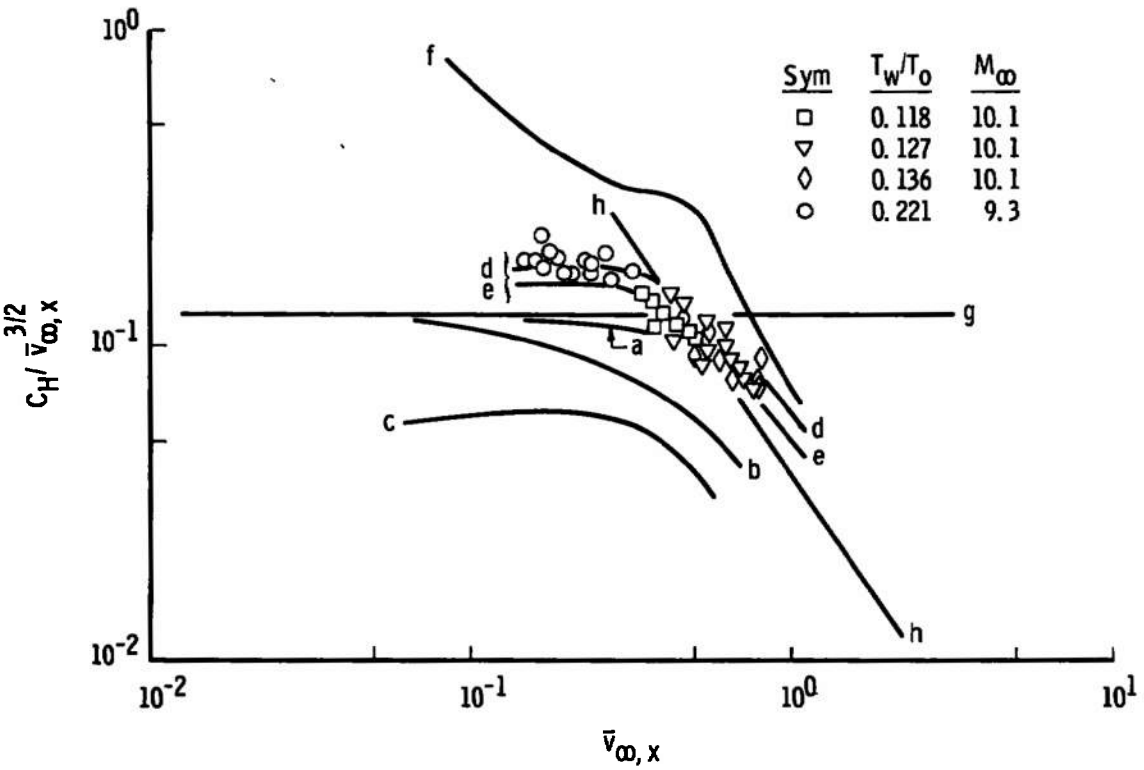

Fig. 16 Comparison of Zero Angle-of-Attack Data with Theoretical Predictions

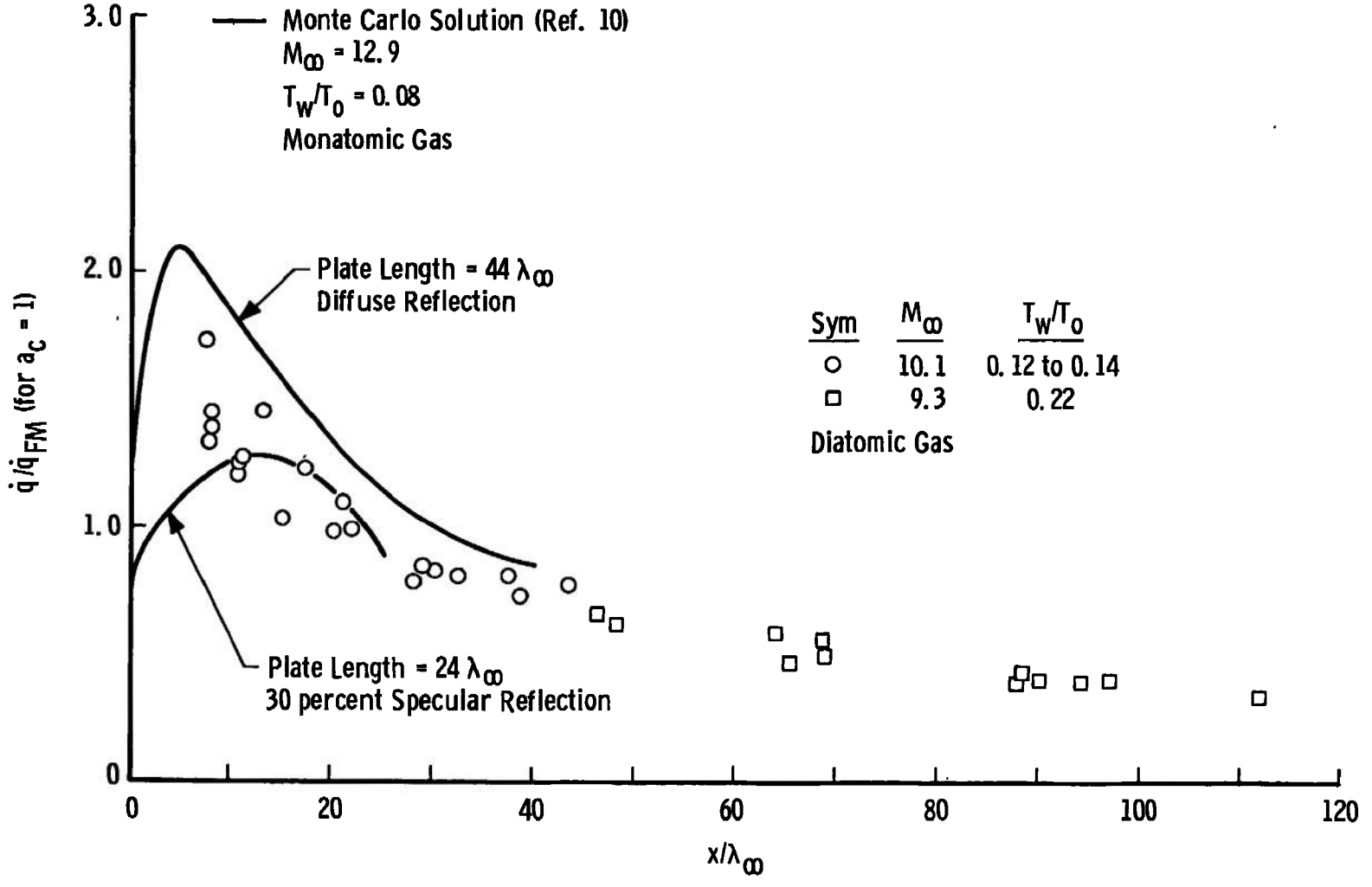

Fig. 17 Comparison of Present Data to Monte Carlo Solution

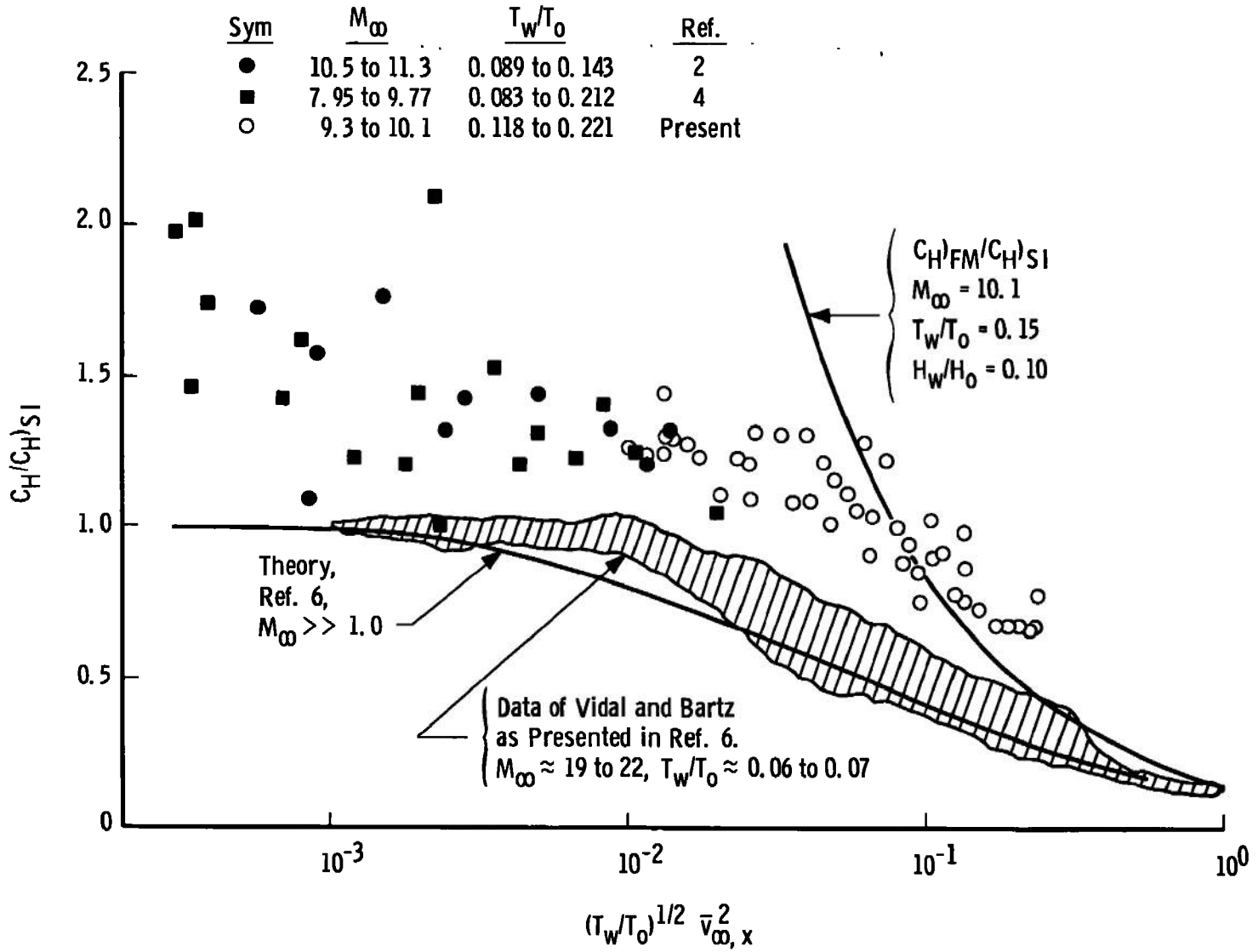

Fig. 18 Comparison of Zero Angle-of-Attack Data at $M_\infty \approx 10$ and $M_\infty \approx 20$

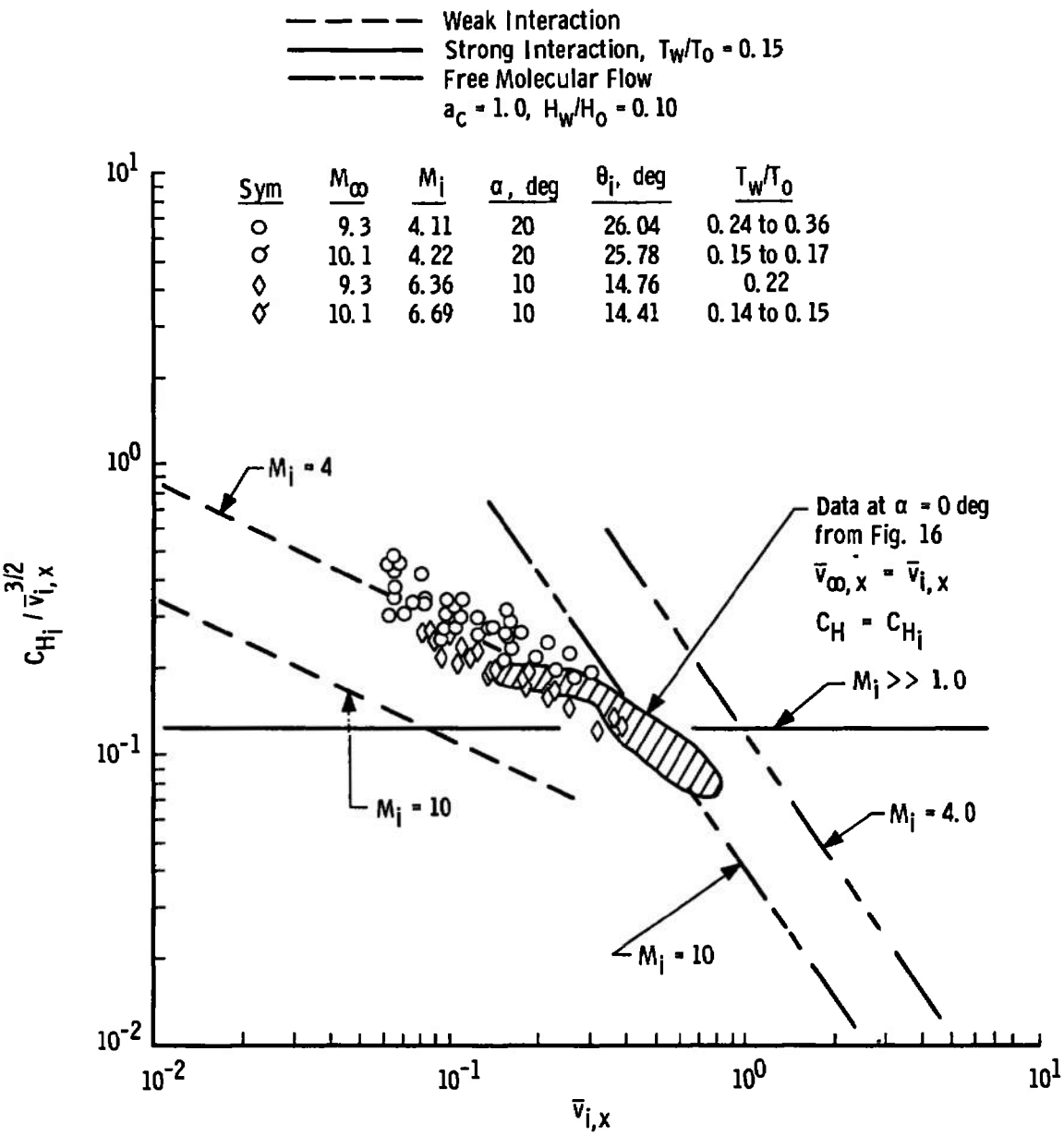

Fig. 19 Heat-Transfer Data at Large Wedge Angles in Terms of Local Inviscid Flow Parameters

TABLE I
FLOW CONDITIONS

Nozzle	10 N_2	9 N_2
M_∞	10.1	9.30
Re_∞, in.$^{-1}$	390	1670
p_o, psia	18	25
T_o, °K	3100	1660
Gas	Nitrogen	Nitrogen
p_∞, μHg	23	50
T_∞, °K	154	94
λ_∞, in.	0.041	0.0083

TABLE II
MATERIAL HEAT-TRANSFER PROPERTIES

Property	Material		
	Nylon	Teflon	Lexan
k, Btu/ft-sec-°R	0.394×10^{-4}	0.389×10^{-4}	0.309×10^{-4}
ρ, lb/ft^3	71.2	137.0	74.9
c, Btu/lb-°R	0.40	0.250	0.30
α' ft^2/sec	0.138×10^{-5}	0.114×10^{-5}	0.138×10^{-5}

TABLE III
CONVENTIONAL GAGES

	Gardon Gage	Slug Calorimeter	Thin-Film Resistance Thermometer
Disk Material	Constantan	302 Stainless Steel	302 Stainless Steel
Disk Thickness, in.	0.001	0.042	0.042
Disk Diameter, in.	0.150	0.187	0.187
Time Response, sec	0.164 (63%)	0.11 (95%)	0.11 (95%)
Calibration Factor, Btu/ft^2-sec/mv	2.381	5.71/sec	0.302/sec

UNCLASSIFIED
Security Classification

DOCUMENT CONTROL DATA - R & D

(Security classification of title, body of abstract and indexing annotation must be entered when the overall report is classified)

1. ORIGINATING ACTIVITY (Corporate author)	2a. REPORT SECURITY CLASSIFICATION
Arnold Engineering Development Center ARO, Inc., Operating Contractor Arnold Air Force Station, Tennessee 37389	UNCLASSIFIED
	2b. GROUP N/A

3. REPORT TITLE

MEASUREMENTS OF LOCAL HEAT-TRANSFER RATE ON A COOLED SHARP FLAT PLATE IN THE MERGED LAYER FLOW REGIME

4. DESCRIPTIVE NOTES (Type of report and inclusive dates)

Final Report August through November 1968

5. AUTHOR(S) (First name, middle initial, last name)

David E. Boylan, ARO, Inc.

6. REPORT DATE	7a. TOTAL NO OF PAGES	7b. NO. OF REFS
June 1969	59	21

8a. CONTRACT OR GRANT NO.	9a. ORIGINATOR'S REPORT NUMBER(S)
F40600-69-C-0001 b. Program Element 65401F	AEDC-TR-69-71
c.	9b. OTHER REPORT NO(S) (Any other numbers that may be assigned this report)
d.	N/A

10. DISTRIBUTION STATEMENT

This document has been approved for public release and sale; its distribution is unlimited.

11. SUPPLEMENTARY NOTES	12. SPONSORING MILITARY ACTIVITY
Available in DDC.	Arnold Engineering Development Center (AETS), Arnold Air Force Station, Tennessee 37389

13 ABSTRACT

Results of measurements of the local convective heat-transfer rate on a sharp-leading-edge flat plate at various angles of attack and in the merged layer flow regime are presented. The measurements were obtained using a phase-change temperature-sensitive paint, which greatly simplifies instrumentation requirements, and these measurements were checked using conventional heat-transfer instrumentation. Data obtained on the windward surface at 0-, 10-, and 20-deg angle of attack are compared to theoretical predictions. The data, which are in the range $0.6 \approx \dot{q} \approx 6.0$ Btu/ft^2-sec, demonstrate the feasibility of utilizing phase-change temperature-sensitive paint in place of conventional heat-transfer instrumentation in low-density high-speed flows. The data at large angles of attack (wedge angles) are shown to correlate in the same manner as the zero angle-of-attack data when local inviscid flow parameters are utilized. Based on local inviscid values, the data are in the Mach number range from 4 to 10 and viscous interaction parameter $\bar{v}_i = M_i(C_i/Re_{i,x})^{1/2}$ range from 0.06 to 0.80. A strong Mach number influence as well as the nonexistence of a definable strong interaction flow regime in this Mach number range was noted.

DD FORM 1 NOV 65 1473

UNCLASSIFIED
Security Classification

14. KEY WORDS	LINK A		LINK B		LINK C	
	ROLE	WT	ROLE	WT	ROLE	WT
heat transfer						
sharp flat plate						
merged layer flow						
temperature sensitive paint						